ARTICLE INFO
Article ID: 04-18-02-0012
2025 Jared Zeman and Adam Dempsey
doi:10.4271/04-18-02-0012

# Mixing-Controlled Combustion of Ethanol Enabled by Prechamber Ignition (PC-MCC): A Preliminary Experimental Demonstration

***Jared Zeman*[1] *and Adam Dempsey*[1]**

[1]*Marquette University, USA*

## Abstract

This experimental study presents preliminary investigations of prechamber-enabled mixing-controlled combustion (PC-MCC) at −2 bar brake mean effective pressure (BMEP) and 2200 rpm with fuel-grade ethanol (E98). Experimental results are conducted on a prechamber retrofitted single-cylinder Caterpillar C9.3B test engine. First, a series of prechamber-only experiments were conducted with a motored engine to evaluate the salient combustion trends in response to relevant prechamber operating parameters. Under firing conditions, the prechamber operating strategy was assessed with respect to the impact on ignition assistance of direct-injected E98 and overall engine performance. The preliminary results indicate the jet-induced ignition process is robust and prompts diffusion combustion of E98 at diesel-like boundary conditions. The effect of external exhaust gas recirculation (EGR) on the residual tolerance of the prechamber combustion process was also investigated and showed stable combustion in both the main chamber and prechamber up to 30% EGR. Experiments were also conducted with the stock diesel engine for baseline comparison. At matched combustion phasing, mixing-controlled combustion of ethanol enabled by prechamber ignition was able to achieve heightened gross thermal efficiency while simultaneously reducing NOx and practically eliminating smoke emissions relative to diesel combustion. In addition, the covariance of load and standard deviation of combustion phasing was diesel-like and less than 2% and 1 CAD, respectively.

### History

Received: 25 Sep 2024
Revised: 26 Nov 2024
Accepted: 26 Feb 2025
e-Available: 17 Mar 2025

### Keywords

PC-MCC, Flex-fuel, Prechamber, Ethanol, Mixing-controlled combustion, Heavy-duty, Single-cylinder

### Citation

Zeman, J. and Dempsey, A., "Mixing-Controlled Combustion of Ethanol Enabled by Prechamber Ignition (PC-MCC): A Preliminary Experimental Demonstration," *SAE Int. J. Fuels Lubr.* 18(2):219–239, 2025, doi:10.4271/04-18-02-0012.

ISSN: 1946-3952
e-ISSN: 1946-3960





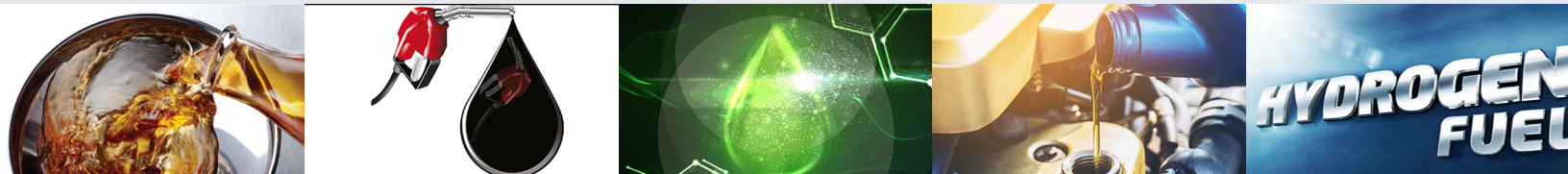

# 1. Introduction

There is an imminent need to develop advanced combustion strategies that allow the use of renewable, low carbon intensity fuels in order to mitigate lifecycle greenhouse gas (GHG) emissions and promote energy sustainability. Combustion of non-renewable fossil fuels, such as diesel, produces harmful pollutants that have adverse effects on human health and overall global climate. The projected increase in energy demand for the heavy-duty energy sector [1] motivates the need to displace the diesel fuel dependency of both on-road and off-road heavy-duty vehicles with clean burning energy sources. Some prime fuel candidates of interest include ethanol, methanol, hydrogen, natural gas, and ammonia, to name a few. Currently, there exist various logistical challenges surrounding the transport and onboard storage of gaseous fuels for the on-road and off-road markets. A more pragmatic approach would be to select fuels that can be easily integrated into the current liquid fuels infrastructure. This work focuses on the use of bioethanol and bioethanol/gasoline fuel blends as an alternative fuel source to help displace fossil fuel dependency on heavy-duty engines. Readily available in the U.S. and foreign markets, e.g., Brazil, and ranging in blends from E10 to E85 and E98, bioethanol is a renewable fuel that demonstrates reductions in lifecycle GHG emissions through its production, distribution, and usage (well-to-wheels) [2]. Dempsey et al. used data from the GREET model [3] to compare a heavy-duty diesel engine to a theorized flex-fuel engine operating at the same brake thermal efficiency and showed that the flex-fuel engine can reduce lifecycle GHG emissions by –10% to –50% when operating on E15 and E98, respectively [4].

The desire to use alternative fuel sources in heavy-duty engines presents a significant challenge—the aforementioned fuels are all poor diesel fuels, i.e., they have a high propensity to resist autoignition. Typical heavy-duty engine architecture is geared toward compression ignition (CI) where reactive direct-injected diesel fuel sprays are ignited in a high-pressure/temperature environment. Direct substitution of liquid fuels such as bioethanol is not plausible as their low reactivities would not constitute the same ignition quality nor achieve autoignition at all. The high octane and volatile nature of these fuels make them well suited for spark ignition (SI) engines; however, SI engines lack the performance characteristics desired for robust heavy-duty operation. Knock is the primary limiting factor to obtain high load at reasonable efficiencies in heavy-duty SI engines. Additionally, SI engines lack good transient snap-torque response due to the fact that they operate stoichiometrically. These operational constraints have inhibited heavy-duty SI engine development outside of constant speed stationary power applications and therefore motivate the use of these fuels in a CI, or mixing-controlled combustion (MCC), manner for mobile applications.

In order to establish MCC with low-reactivity fuels, some form of ignition assistance is required. Some examples of thermal ignition assistance devices and methodologies include the use of continuously powered glow plugs [5–9], high compression ratio [10, 11], uncooled EGR [12, 13], variable valve strategies [14, 15], reactivity and thermal stratification [16–23], and thermal barrier coatings [13, 24–26], among others. Recent works have focused on the forced interaction of the direct-injected fuel with a high temperature ignition source in the form of a burning jet or reacting fuel plume to prompt immediate ignition and subsequent diffusion combustion. Non-premixed dual-fuel combustion systems [27–30] utilize a dedicated direct injector to deliver a pilot injection of high-reactivity fuel, e.g., diesel, as the ignition source. The pilot readily ignites, and the burning fuel plumes are strategically aligned with the main injection to ensure strong flame–spray interaction to induce ignition. Non-premixed dual-fuel engines enable MCC of low-cetane fuel sources but have practical limitations associated with the cost and complexity of incorporating two separate high-pressure fuel systems. Space constraints and accessibility to varying fuel streams are also limitations. The desire to eliminate the need for two separate fuel streams of varying reactivity but maintain the ignition capabilities of a flame-induced ignition system prompted Kammel et al. [31] and Zelenka et al. [32] to demonstrate the use of an actively fueled prechamber (PC) to ignite a high-pressure direct injection (HPDI) of natural gas in a non-premixed large bore engine. The annulus-style PC is centrally mounted with the HPDI injector and is responsible for producing hot turbulent jets that are closely coupled with the direct injection event such that injected fuel is quickly impinged by the aligned hot jets, prompting immediate diffusion combustion and thus robust control of combustion. This concept was extended to pure ethanol and methanol by Dempsey et al. [4, 33] with a similar annulus-style active PC and center-bore injector configuration. The numerical results demonstrated the robustness of jet-induced ignition aid for high-pressure liquid fuels and the ignition concept was termed prechamber-enabled mixing-controlled combustion, or PC-MCC.

Recent PC-MCC modeling efforts by Zeman et al. [34–36] have since incorporated a MAHLE jet ignition (MJI)-style PC to the ignition concept. The generalized PC-MCC ignition process with an offset MJI igniter and E98 fuel is illustrated in Figure 1 relative to conventional diesel combustion (CDC). Early in the compression process, the PC is actively fueled with an integrated injector as air from the main chamber (MC) is pushed into the PC by piston motion. An ignitable mixture is formed in the PC near the top dead center (TDC) and the charge is ignited with a spark plug. The small volume combusts rapidly, producing hot turbulent jets that penetrate the MC and impinge upon the direct-injected fuel, prompting immediate ignition. Recent research has focused on the

**FIGURE 1** Pictorial representation of the prechamber ignition concept, or PC-MCC (bottom row), with ethanol fuel relative to diesel combustion (top row). Iso-surfaces depict local gas temperature. Fuel parcels are depicted with black droplets.

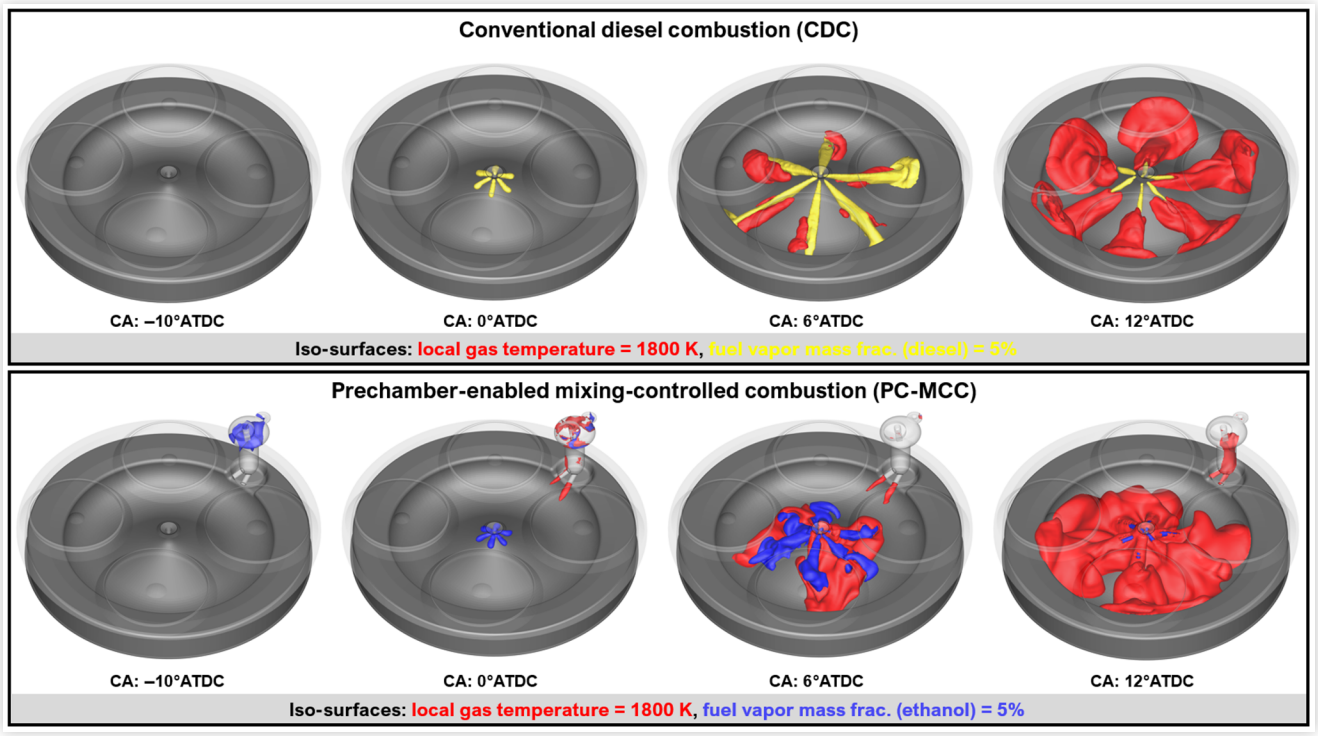


Jared Zeman and Adam Dempsey

technological development of the ignition concept, assessing the salient design features (igniter location, volume, hole size, number of holes, hole angles, etc.) and operating strategies for robust ignition performance. Relying on the numerical results, a prototype MJI was developed and retrofitted to a production Caterpillar C9.3B cylinder head for single-cylinder PC-MCC engine testing. This work serves as the first experimental demonstration of PC-MCC with E98 fuel following the numerical proof of concept and strategy development.

# 2. Materials and Methods

## 2.1. Experimental Single-Cylinder Test Engine

In this study, experiments are conducted on a single-cylinder heavy-duty CI test engine. The test engine is based on a Caterpillar C9.3B inline-six heavy-duty diesel engine and was converted to single-cylinder operation by deactivating cylinders 1–5, leaving cylinder 6 as the active firing cylinder. The relevant specifications of the engine are shown Table 1. The stock Caterpillar C9.3B high-pressure fuel system is a Bosch common rail injection system (CRS) that utilizes a gear-driven high-pressure pump and side-feed/in-head fuel return-style solenoid injectors. The single-cylinder test engine utilizes the stock high-pressure fuel delivery system while the low-pressure system, i.e., supply and return, is purpose-built to handle low- and high-volatility fuels. The return fuel from the CRS needs to be at low pressure (<0.5 bar-g) to minimize backpressure on the injector but is at a relatively high temperature (–50°C to 60°C) from in-head return. The

**TABLE 1** Specifications of single-cylinder test engine based on Caterpillar C9.3B.

| **Engine specification** | | **Value** |
|---|---|---|
| Engine type | | Four-stroke |
| Piston material | | Aluminum |
| Combustion system | | Deep spray angle |
| Bore | [mm] | 115 |
| Stroke | [mm] | 149 |
| Connecting rod | [mm] | 217 |
| Displacement | [L] | 1.55 |
| Compression ratio | [-] | 17 |
| Clearance volume | [$cm^3$] | 96.88 |
| Intake valve open/close | [°ATDC] | 350.4/–152.5 |
| Exhaust valve open/close | [°ATDC] | 135.6/–339.5 |
| **MC fuel system specification** | | **Value** |
| Injection system | | Common rail |
| Injector umbrella angle | [°] | 135 |
| Number of holes | [-] | 6 |
| Hole diameter | [µm] | 205 |
| Rated injection pressure | [MPa] | 250 |

Jared Zeman and Adam Dempsey

low-pressure fuel system is designed to manage cooling of the return fuel from the CRS while allowing metered makeup fuel into the system, which represents the amount of fuel delivered by the common rail injector. To avoid any potential vaporization, the return fuel is cooled to –20°C before being mixed with metered makeup fuel. The makeup fuel is measured by an Endress and Hauser Promass 83A02 Coriolis flowmeter.

The single-cylinder engine's air and exhaust systems are configured to simulate turbocharging with high-pressure loop EGR. The air handling system is extremely flexible and can independently set intake and exhaust pressures and EGR flowrate with electronic actuators. The intake air is supplied by a 60 hp rotary screw air compressor with an integrated refrigeration drying system. The air is relatively dry with an absolute humidity of <1 g-$H_2O$/kg-air. The intake air is heated with a single-pass 16-kW circulation heater. The intake air and EGR mass flow rates are measured with Endress and Hauser Promass 83F Coriolis flowmeters.

PC-MCC experiments were conducted on the test engine using a prechamber retrofitted cylinder head. The retrofitted head was developed to be non-invasive to the stock valve actuation mechanism and CRS allowing for adequate comparisons to CDC with the stock cylinder head. A cross-sectional view of the modified cylinder head and PC assembly is depicted in Figure 2. The PC design is based on a MAHLE turbulent jet ignition system and its relevant design features and hardware are listed in Table 2. The PC utilizes a specially designed gasoline direct injection (GDI)-style injector to meter small quantities of fuel. The injector is supplied with pressurized fuel from a $N_2$ gas-charged piston accumulator. The injection pressure in the PC is set by regulating the $N_2$ gas supply to the desired operating pressure. An Endress and Hauser Proline Promass A 500 Coriolis flow meter is used to measure steady-state fuel flow for shot mass prediction. A Kistler 6113C pressure measuring spark plug (MSP) is used to initiate combustion in the PC and provide crank angle-resolved pressure data for analysis.

As depicted in Figure 3, the PC is mounted at the periphery of the combustion chamber with its orifices directed toward the center of the chamber. When ignited, hot turbulent jets emanate from the PC and penetrate toward the center of the combustion chamber to ignite the direct-injected fuel. The PC nozzle protrudes approximately 5 mm from the fire deck and thus requires a relief cut in the piston lip. With the additional volume of the PC and dead volume between the piston relief cut and the PC nozzle, the stock compression ratio of 17.0:1 was estimated to be reduced to –16.4:1.

**TABLE 2** Prechamber specifications.

| PC specification | | Value |
|---|---|---|
| Prechamber design | | MAHLE Active MJI® |
| Mounting configuration | | Side mount |
| Fueling system | | Piston accumulator |
| Spark plug | | Kistler 6113C MSP |
| Ignition coil | | MSD smart coil |
| Volume | [$cm^3$] | 2 |
| # of orifices | [-] | 2 |
| Orifice diameter | [mm] | 2.3 |
| Orifice span angle | [°] | 30 |
| Orifice umbrella angle | [°] | 145 |
| **PC injector specification** | | **Value** |
| Injector style | | GDI |
| Spray angle from principal axis | [°] | 40 |
| Number of holes | [-] | 1 |
| Hole diameter | [μm] | 120 |
| Rated injection pressure | [bar] | 350 |

Jared Zeman and Adam Dempsey

**FIGURE 2** Prechamber and cylinder head assembly cross-sectional view.

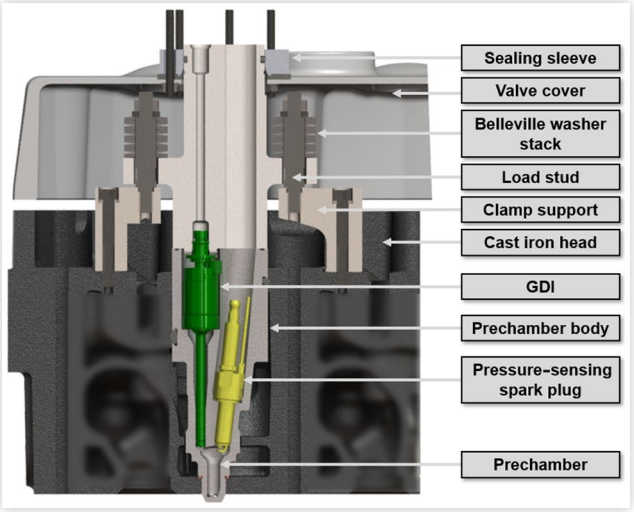


Jared Zeman and Adam Dempsey

## 2.2. Emissions Sampling and Data Acquisition

Gaseous exhaust emissions were measured with an MKS 2030 Fourier transform infrared (FTIR) spectrometer. MKS data analysis software MG2000 was used to identify and measure the volumetric concentration of select gas phase species—NO, $NO_2$, CO, $CO_2$, $H_2O$, and select hydrocarbon species. Exhaust oxygen was measured with a Horiba MEXA-730λ with a UEGO sensor. Total unburned hydrocarbons were measured with a California Analytical Instruments heated flame ionization detector (HFID). The exhaust sample stream was conveyed from a heated filter to the FTIR and HFID through heated lines maintained at 190°C. Black carbon soot emissions were measured with an AVL 415SE Smokemeter. The results from the smokemeter measurements will be presented as filter smoke number (FSN).

**FIGURE 3** PC-MCC combustion chamber and depiction of ignition concept.

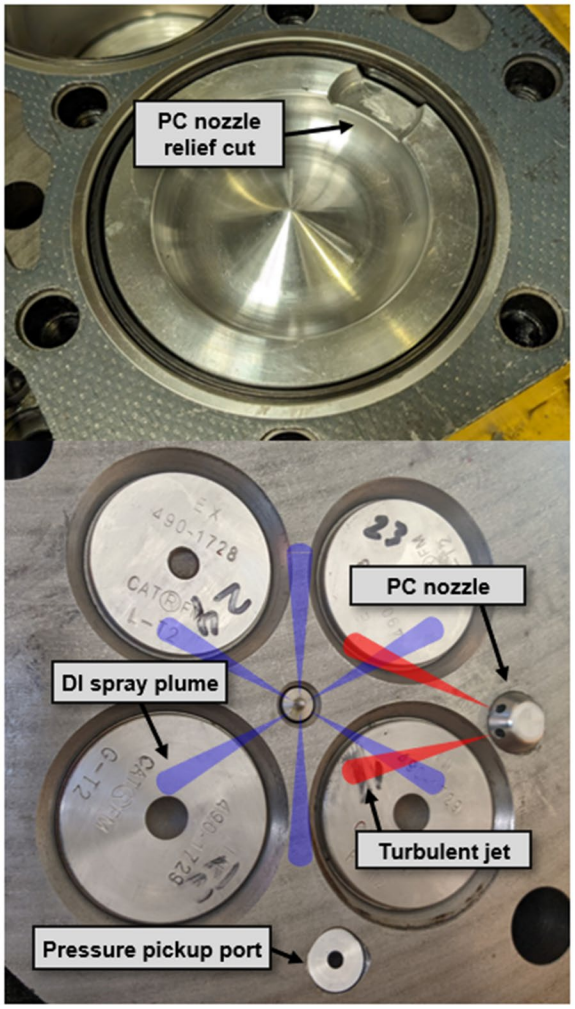


Jared Zeman and Adam Dempsey

The stock engine control unit was replaced with a full-pass control system from National Instruments—Powertrain Controls Group, which allowed synchronous control of the common rail injector, PC injector and spark plug, and all other relevant engine position-based laboratory actuators. High-speed in-cylinder pressure data was acquired using a Kistler model 6124A piezoelectric pressure transducer and a Kistler type 5064 charge amplifier. The 6124A was mounted in a recessed position to protect the transducer from thermal shock [37]. Crank shaft position was measured with a Kistler 2614C encoder with a sampling resolution of 0.1 crank angle degrees (CAD). The intake and exhaust runner pressures are synchronously measured as a function of crank angle using Kistler 4007A piezoresistive pressure transducers. High-speed data (i.e., in-cylinder pressure, runner pressures, injector current traces, etc.) was recorded for 300 consecutive engine cycles. The low-speed data (airflow, fuel flow, boundary conditions, and emissions) were recorded for 60 s at 10 Hz. The individual cycle cylinder pressure traces are digitally filtered to remove high-frequency noise and allow for interpretable heat release analysis. A Fourier series band-pass filter with a Gaussian roll-off function used by Higgins and Siebers was used in this work [38]. The filter has a transmission of 100% from 0 kHz to 2 kHz and dropping to 1% transmission at 5 kHz, and thus is a form of low-pass filter. Once each cycle is pegged and filtered, the cylinder pressure data is ensemble averaged to yield a representative cylinder pressure trace.

## 2.3. Apparent Heat Release Analysis

First-law analysis of a closed piston-cylinder system with the standard assumptions that the chamber contents obey the ideal gas law, there is no mass loss (blowby), and potential and kinetic energy losses are negligible, the standard expression for the apparent heat release rate (AHRR), i.e., chemical energy release minus heat transfer losses, can be derived as

$$\frac{dQ}{d\theta} = \frac{\gamma}{\gamma - 1} P \frac{dV}{d\theta} + \frac{1}{\gamma - 1} V \frac{dP}{d\theta} \tag{1}$$

where $P$ is the chamber pressure, $V$ is the chamber volume, and $\gamma$ is the specific heat ratio of the chamber contents. The addition of an auxiliary chamber confounds the traditional single-zone first-law analysis to calculate the AHRR for combustion analysis. The two chambers exchange mass during compression, combustion, and expansion, thus the first-law analysis must be updated to account for two open systems connected via orifices. As such, the apparent heat release in the MC and the PC can be calculated. For the sake of brevity, the derivation for this system will not be given here as it is outlined in detail by Heywood [39]. The respective AHRRs for the MC and PC are

$$\frac{dQ_{MC}}{d\theta} = \frac{\gamma}{\gamma - 1} P_{MC} \frac{dV_{MC}}{d\theta} + \frac{1}{\gamma - 1} V_{MC} \frac{dP_{MC}}{d\theta} - c_p T \frac{dm}{d\theta} \tag{2}$$

$$\frac{dQ_{PC}}{d\theta} = \frac{1}{\gamma - 1} V_{PC} \frac{dP_{PC}}{d\theta} + c_p T \frac{dm}{d\theta} \tag{3}$$

where $m$ is the mass exchanged between the chambers and $c_p$ and $T$ are the heat capacity and temperature of the gas exchanged between the chambers, respectively. The mass exchange rate is defined to be positive when flowing from the PC to the MC. Depending on which direction the flow is, the heat capacity and temperature need to be updated to represent the enthalpy flux from the appropriate chamber. For example, during compression, MC gases are pushed in the PC, thus the mass flow rate is negative and $c_p$ and $T$ are equated to the MC values. Using the ideal gas law to determine the

respective chamber temperatures, the specific heat capacities can be determined by trapped mass mixture fractions of global combustion reactants and products.

The mass exchange rate between the two chambers is governed by the relations for isentropic compressible flow through a restriction, i.e., an orifice(s),

$$\frac{dm}{d\theta} = C_d \frac{AP_0}{\sqrt{R_{gas}T_0}} \left(\frac{P}{P_0}\right)^{\frac{1}{\gamma}} \sqrt{2\frac{\gamma}{\gamma-1}\left[1-\left(\frac{P}{P_0}\right)^{\frac{\gamma-1}{\gamma}}\right]} \quad (4)$$

where $C_d$ is the discharge coefficient, $A$ is the total area of the orifices, and the subscript naught refers to the stagnation, or upstream, conditions. For example, for flow from the MC into the PC, the pressure and temperature in the MC are the stagnation (upstream) conditions and the pressure in the PC is the downstream condition. If the flow between the two chambers exceeds the critical pressure ratio

$$\frac{P}{P_0} \leq \left(\frac{2}{\gamma+1}\right)^{\frac{\gamma}{\gamma-1}} \quad (5)$$

then the flow becomes choked. Under choked flow, the mass exchan ge rate reduces to

$$\frac{dm}{d\theta} = \frac{AP_0\sqrt{\gamma}}{\sqrt{R_{gas}T_0}} \left(\frac{2}{\gamma+1}\right)^{\frac{\gamma+1}{2(\gamma-1)}} \quad (6)$$

In this study, the discharge coefficient is assumed to be constant and is tuned to match the mass flow rate predictions from available CFD data. The discharge coefficient is expected to change with varying PC geometries and thus must be assessed with 1D or 3D modeling efforts to match the specific application. In other PC AHRR works, the discharge coefficient is quoted to be anywhere from 0.3 to 0.6 [40, 41], which supports the value of 0.45 used in this study. A more detailed approach by Balmelli et al. [42] updates the discharge coefficient on cycle basis to ensure appropriate predictions of chamber mass (and thus temperature by use of the ideal gas law) before and after combustion.

Inspection of (2) and (3) relative to (1) reveals that the only differences are the added enthalpy flux terms and the change in volume for (3) is neglected as the chamber volume is fixed. The enthalpy flux terms are relatively small during the closed cycle and are only significant during PC combustion. Figure 4 demonstrates the PC and MC AHRR determination relative to traditional single-zone analysis. Firing pressure traces for both chambers, motoring pressure in the MC, electronic commanded injection, and hydraulic rate of injection (ROI) are provided

**FIGURE 4** Comparison of single- and dual-zone AHRR traces for PC-MCC combustion with E98 fuel.

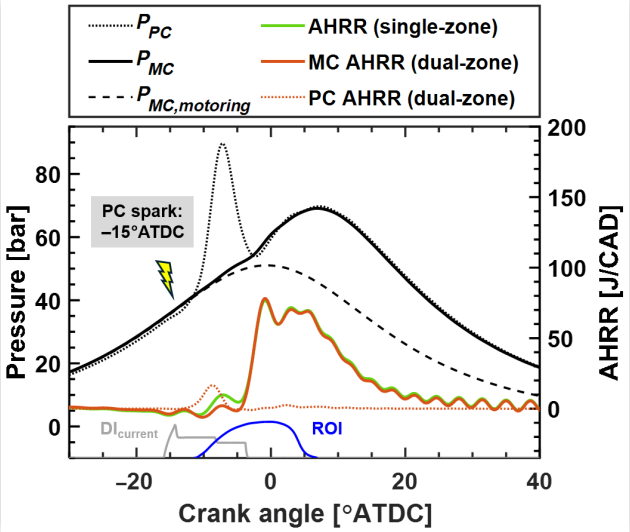


Jared Zeman and Adam Dempsey

for reference. As illustrated in Figure 4, the commanded start/end of injection (injector current profile) and actual start/end of hydraulic injection are different quantities and vary based on injector configuration, fuel properties, and injection pressure, among other factors. For the injector used in this study, the estimated opening and closing delay at the specified injection pressures is roughly 4.5 CAD and 11.5 CAD, respectively. These values were estimated using diesel fuel and it is unknown how the fuel properties of ethanol will change these values; however, it is expected that they will be similar.

Shortly after the commanded PC spark timing of –15°ATDC, the PC pressure rises rapidly, and the associated PC AHRR is shown. The PC combustion produces hot jets that penetrate the MC quickly, and the MC pressure rises slightly from the reference motored value due to the rapid mass addition and any exothermic effects associated with the jets (i.e., reacting jets). After an ignition delay of –5 CAD, the jets induce simultaneous combustion of the injected fuel plumes as denoted by a rapid premixed burn spike that soon transitions to rate-limited combustion with E98 fuel. The peak rate of combustion occurs near the end of injection as expected and is followed by a short late-cycle burn associated with diffusion combustion of oxygenated fuels [43]. Comparison of the single-zone and dual-zone MC AHRR traces shows that the associated enthalpy flux correction during PC jet ejection is the only noticeable difference between the two methodologies.

## 2.4. Operating Conditions

The operating conditions for PC-MCC investigated in this study are based on a hard-to-ignite scenario of –2 bar BMEP and 2200 rpm with fuel-grade ethanol (E98). The

**TABLE 3** PC-MCC operating parameters.

| Parameter | | Value |
|---|---|---|
| Fuel (MC & PC) | | E98 |
| Engine speed | [rev/min] | 2200 |
| Load (gross/brake) | [bar] | 4.5/2 |
| CA50 timing | [°ATDC] | Varies |
| EGR % | [-] | 0 to 35 |
| Coolant temperature | [°C] | 87 |
| Intake temperature | [°C] | 50 |
| Intake pressure | [bar] | 1.2 |
| Exhaust pressure | [bar] | 1.3 |
| MC injection strategy | | Single injection |
| MC injection timing | [°ATDC] | Varies |
| Rail pressure | [bar] | 750 to 1000 |
| PC injection timing | [°ATDC] | −240 to −60 |
| PC injection pressure | [bar] | 130 |
| PC elec. injection duration | [ms] | 2 to 6 |
| PC spark timing | [°ATDC] | −26 to 6 |
| PC spark dwell duration | [ms] | 4 |

relevant boundary conditions and injection strategies are summarized in Table 3. The boundary conditions are selected to be representative of the conditions produced by the air handling system of a conventional turbocharged diesel engine. In this study, a variety of parametric studies surrounding the PC operating strategy were assessed. First, a series of PC-only experiments, i.e., no MC injection, were conducted to characterize the PC fuel preparation strategy and subsequent combustion process. Feedback from PC pressure (variance and peak magnitude) and engine-out emissions measurements (unburned fuel and NO) were used to identify combustion stability and ignitability trends. After assessing the PC combustion process, the MC direct injection of E98 was introduced and the ignition quality was evaluated under different operating strategies, namely the impact of PC stoichiometry, PC spark timing, and MC DI timing.

Next, external EGR was introduced to observe the residual tolerance of the PC combustion and its impact on ignition performance. Historically, both conventional CI and SI combustion systems have used EGR to help mitigate NOx emissions by lowering combustion temperatures. Typical diesel combustion systems can typically withstand up to 50% EGR whereas SI engines are generally limited to 30%. The differences in residual tolerances stem from the rudiments of both respective combustion systems. High amounts of residual concentration in SI engines dramatically slows the premixed air–fuel flame speed and results in high cyclic variability and increased UHC emissions. Conversely, diesel engines operate globally lean and establish heterogeneous combustion in a rate-limited mixing process where the main limitation to excessive EGR rates is elevated soot production due to high localized equivalence ratios. PC-MCC is an agglomeration of both CI and SI engine architectures—the MC representative of diffusion-style combustion system and the PC a premixed spark-initiated combustion system. For this reason, it is of interest to quantify the residual tolerance of the PC by using external EGR and evaluate the corresponding implications on the jet-induced ignition process.

Lastly, engine performance, combustion stability, and emissions were evaluated relative to diesel combustion over a range of matched combustion phasing.

# 3. Results and Discussion

## 3.1. Assessment of Prechamber Operation

It is of interest to first evaluate the PC fueling strategy and subsequent PC combustion trends such that the best mixture preparation practices can be identified and exercised throughout the remainder of this work. In other words, a pseudo-determination of PC stoichiometry and mixture quality is needed prior to any evaluation of the ignition assistance provided by the PC. To do so, the test engine was motored and only the PC was fired such that pressure and emissions measurements can be used to evaluate the PC combustion. It is expected that near stoichiometric operation produces stable PC combustion and minimal raw fuel slip. Conversely, rich and lean conditions are expected to produce variable PC combustion with low NO emissions and heightened raw fuel emissions due to poor or incomplete combustion. NO emissions are expected to peak slightly lean of stoichiometric ($\phi$−0.9) [39].

First, the impact of PC fuel shot quantity was evaluated by varying the commanded electronic injection duration and measuring the steady-state fuel flow. The commanded start of PC injection (SOIc) and spark timing were fixed at −120°ATDC and −15°ATDC, respectively. The resultant combustion processes are observed in the PC pressure traces provided in Figure 5 and emissions measurements in Figure 6. Under lean conditions, the PC lacks appreciable pressure buildup and has significant ethanol slip and low NO production. As the fuel quantity increases from lean, the combustion process becomes more repeatable, and NO production steadily rises until it peaks at near stoichiometric proportions. Further enrichment to the PC reduces NO production and slightly increases ethanol slip while the combustion process becomes more erratic in phasing and peak magnitude. As expected, carbon monoxide (CO) steadily climbs as the mixture becomes increasingly rich due to incomplete oxidation. Once the PC combustion contents are ejected into the MC, any post-combustion oxidation of unburned hydrocarbons (UHC) or CO is effectively eliminated as the relatively cold bulk gas temperature freezes the kinetic reaction rates. Across the range in air–fuel mixtures

**FIGURE 5** Cycle average (solid black) and individual cycles (gray) of PC pressure from lean to rich operating conditions. PC spark timing is –15°ATDC.

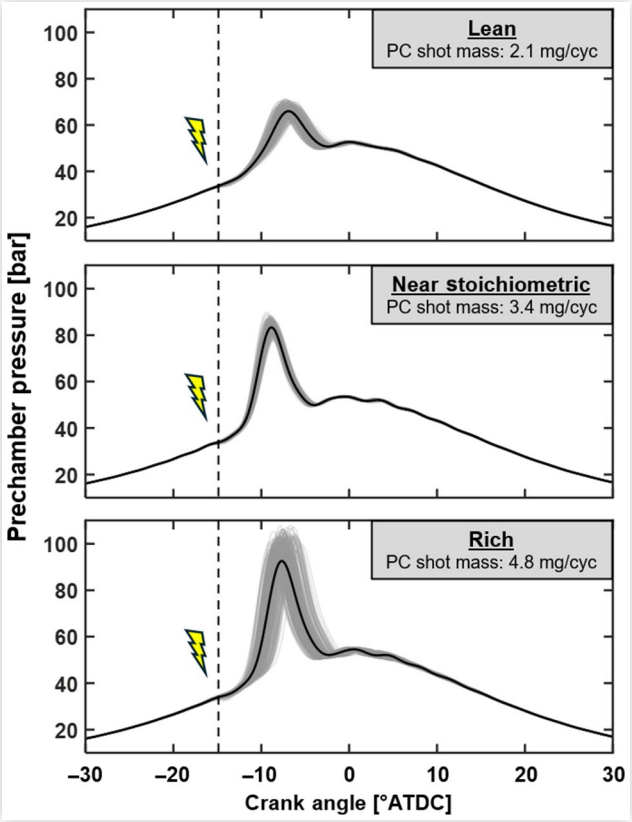


considered, a minimal ethanol slip of –80 ppm is observed, indicating an indefinite source of combustion inefficiency regardless of PC stoichiometry.

Potential sources of PC combustion inefficiencies include incomplete evaporation of fuel films that develop during the PC spray-mixing process, near-wall or crevice flame quenching, local mixture stratification (rich pockets), raw fuel "blow through" during the injection process, or a "cool jet" ejection of unburned charge ahead of the expanding gases in the early stages of PC combustion [36, 44, 45]. The cool jet phenomenon is less of a concern for conventional PC SI applications because the unburned charge mixes into a premixed air–fuel environment that subsequently burns. In this context, the cool jet penetrates into predominantly air (and diluent, if present) thus leaning out rapidly. Following ejection, it is uncertain whether the cool jet is combusted at the head of the penetrating jet or subsequently mixes out and leads to UHC emissions.

Next, the PC SOIc timing was varied under a fixed fuel flow of 3.5 mg/cyc achieved with a commanded 4 ms electronic duration. Again, the spark timing was fixed at –15°ATDC. The resultant combustion processes are observed in the PC pressure traces provided in Figure 7 and emissions measurements in Figure 8. To supplement the findings, the approximate end of injection based on

**FIGURE 6** Raw ethanol, carbon monoxide, and nitric oxide emissions over a range of measured PC fuel shot quantities. Carbon monoxide is scaled down by half for visualization purposes.

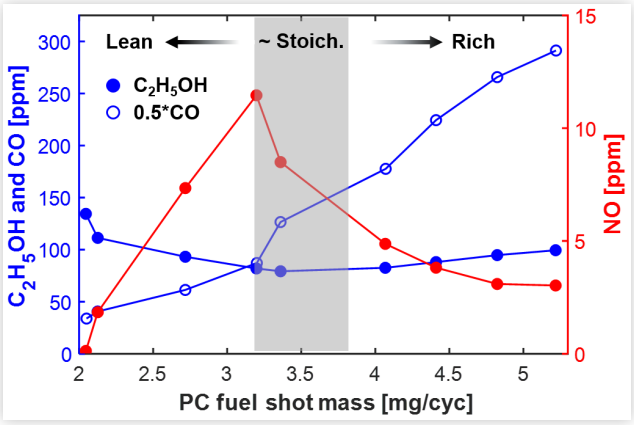


the electronic injection duration is provided in Figure 8. It should be noted that the electronic injection duration of 4 ms is roughly 53 CAD at 2200 rpm; however, the hydraulic injection duration, i.e., actual liquid injection duration, is likely longer due to nonlinear injector behavior at needle opening and closing.

At early injection timings, i.e., before bottom dead center (BDC) of the compression stroke, the injected fuel is prone to blow through into the MC as indicated by the rise in ethanol slip and slow combustion process (lean). As the piston rounds BDC and the compression stroke begins, a concentrated flow of fresh air into the PC is established by upward piston motion that abates fuel blow through. Further reductions in fuel blow through are achieved leading up to and just after inlet valve closure (IVC) as the conditions inside the PC encourage better fuel atomization and mixing upon injection. As a result, the PC combustion process improves, as indicated by the stable PC combustion and reduced ethanol slip. As the injection timing becomes excessively retarded, the available time for air–fuel mixing prior to ignition timing becomes increasingly short and the combustion process rapidly deteriorates due to the high degree of mixture stratification. PC combustion was not achievable with injection timings later than –50°ATDC. Based on these results, the optimal injection timings are early in the compression process shortly after IVC in which ample mixing time and sufficient bulk gas motion into the PC are achieved for adequate mixture preparation.

Lastly, the transient evolution of the mixture stoichiometry was investigated by varying the spark timing under fixed PC fueling conditions. The resultant combustion processes are observed in the PC pressure traces provided in Figure 9 and emissions measurements in Figure 10. At the earliest spark timing of –30°ATDC, the PC combustion process is erratic, and the onset of PC combustion significantly lags the commanded timing. This

**FIGURE 7** Cycle average (solid black) and individual cycles (gray) of PC pressure from under different PC injection timings. PC spark timing is –15°ATDC.

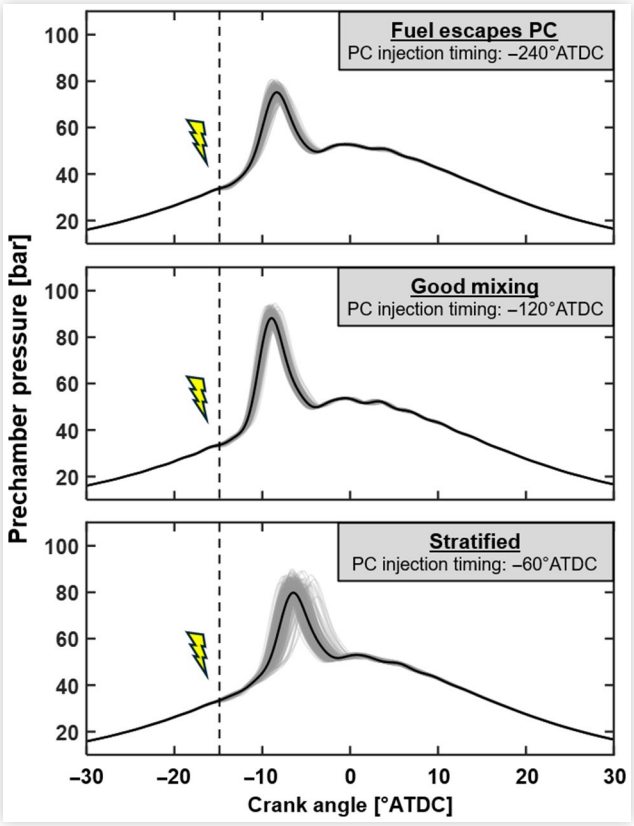


Jared Zeman and Adam Dempsey

**FIGURE 9** Cycle average (solid black) and individual cycles (gray) of PC pressure from under different PC spark timings under fixed fueling.

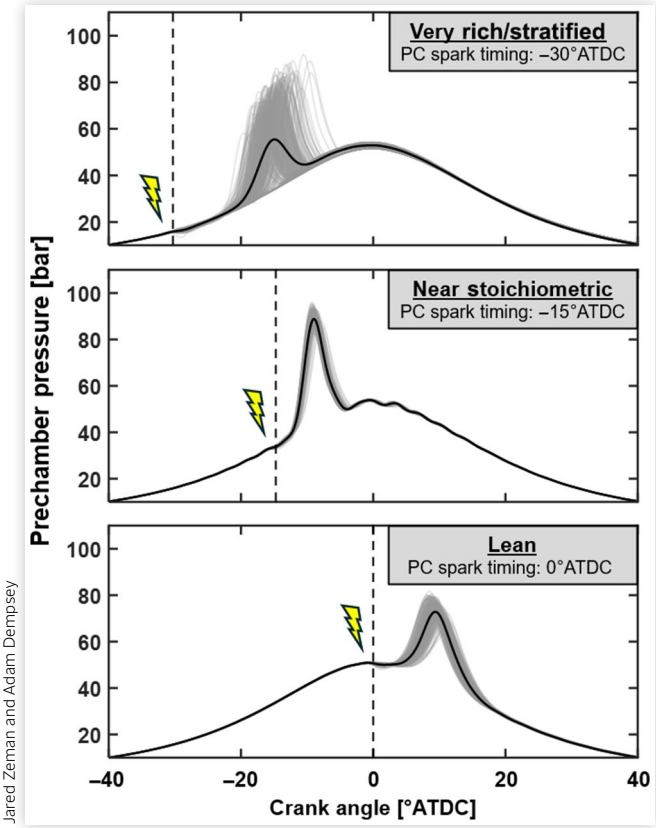


Jared Zeman and Adam Dempsey

**FIGURE 8** Raw ethanol and nitric oxide emissions over a range of PC commanded start of injection timings.

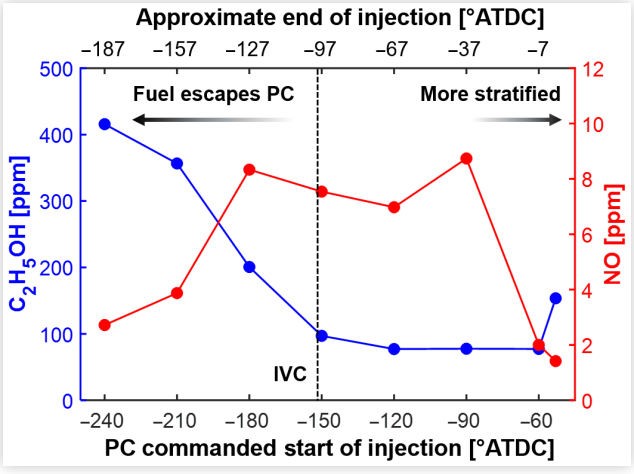


Jared Zeman and Adam Dempsey

**FIGURE 10** Raw ethanol, carbon monoxide, and nitric oxide emissions over a range of PC spark timings under fixed fueling.

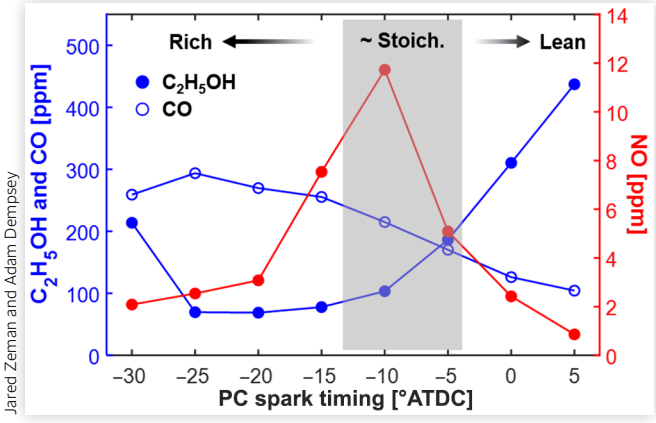


Jared Zeman and Adam Dempsey

is indicative of a rich mixture that likely has a higher degree of local mixture stratification due to a lack of mixing time. As the spark timing is retarded by 15 CAD, the concentration of air in the PC substantially increases and the overall mixing time improves, thus enhancing the combustion process. As the timing continues to retard, the air concentration within the PC continues to increase and subsequently leans out of the mixture. Heightened ethanol slip is observed at the latest spark timings, likely explained by the reversal in flow direction between the two chambers as the piston stagnates near the end of the compression stroke and begins the expansion stroke. This reversal in flow effectively draws out unburned charge from the PC before combustion. In addition, the cool jet effect of unburned charge being ejected ahead of an expanding flame front is also likely amplified at late timings as there is less resistance from air motion into the PC. The distinct transient evolution of mixture quality is a consequence of having a high compression ratio engine in which the air density within the PC changes significantly as a function of crank angle. This effect will be further amplified at boosted conditions. These results indicate that the PC fueling quantity must be appropriately calibrated to the relevant firing conditions within the PC.

## 3.2. Evaluation of PC Operating Strategy

In this section, the HPDI of E98 in the MC is introduced, and its ignition quality is evaluated under varying operating strategies. The parameters of interest include PC shot mass, i.e., PC stoichiometry, and the relative timing split between the main injection timing and PC spark timing. This timing split is achieved by fixing the injection timing while varying the spark timing and vice versa. For the remainder of the study, the PC injection timing and injection pressure remain fixed at –120°ATDC and 130 bar, respectively.

First, the impact of PC shot mass was evaluated at fixed spark and MC DI timing of –15°ATDC and –16°ATDC, respectively. The subsequent ignition performance achieved from lean to rich PC operation is observed in Figures 11 and 12. Under lean PC conditions (<3 mg/cyc), the ignition quality is poor, leading to unstable combustion with high UHC and CO emissions. The ignition quality improves significantly as the PC approaches slightly rich to rich conditions (>4 mg/cyc).

The cycle-to-cycle variations in both chambers from lean to rich PC conditions are presented in Figure 13. As expected from Figure 5, it is observed that rich PC operation results in high cyclic variability yet demonstrates the most stable and advanced MC combustion. Despite the quality of ignition observed, CO and UHC emissions begin to rise as the PC approaches rich conditions. This indicates the subtle rise in emissions under rich PC operation likely comes from the PC itself as observed by the rise in CO and ethanol slip in Figure 6. Not included in Figure 6 is any non-ethanol PC-out hydrocarbons as a result of incomplete combustion that would contribute to the total UHC reported in Figure 12. The trends in ignition performance with PC stoichiometry are supported by a recent numerical work by Zeman et al. [36], which demonstrated rich PC operation is favorable due to the production of reacting jets that elevate in temperature as they

**FIGURE 11** PC shot mass sweep under fixed direct injection conditions. PC spark timing and commanded direct injection timing are –15°ATDC and –16°ATDC, respectively.

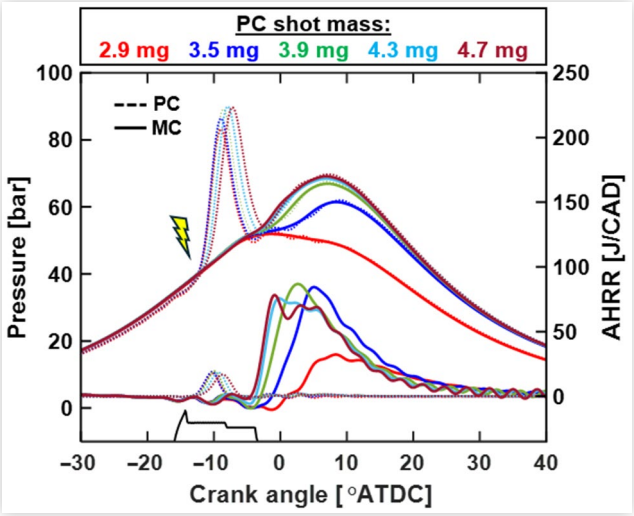


Jared Zeman and Adam Dempsey

**FIGURE 12** Emissions and engine performance trends with respect to changes in PC shot mass.

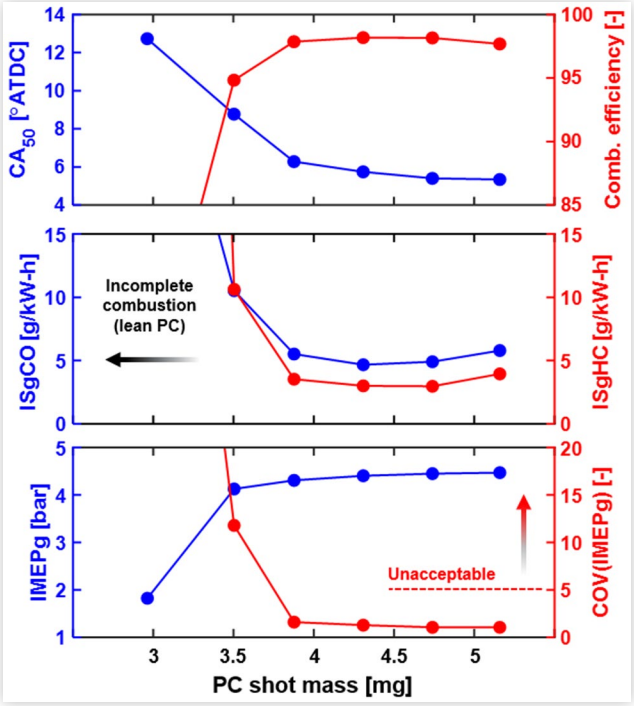


Jared Zeman and Adam Dempsey

**FIGURE 13** MC (blue) and PC (red) ignition quality trends for PC-MCC. Colored lines denote ensemble average and gray lines denote individual measured cycles.

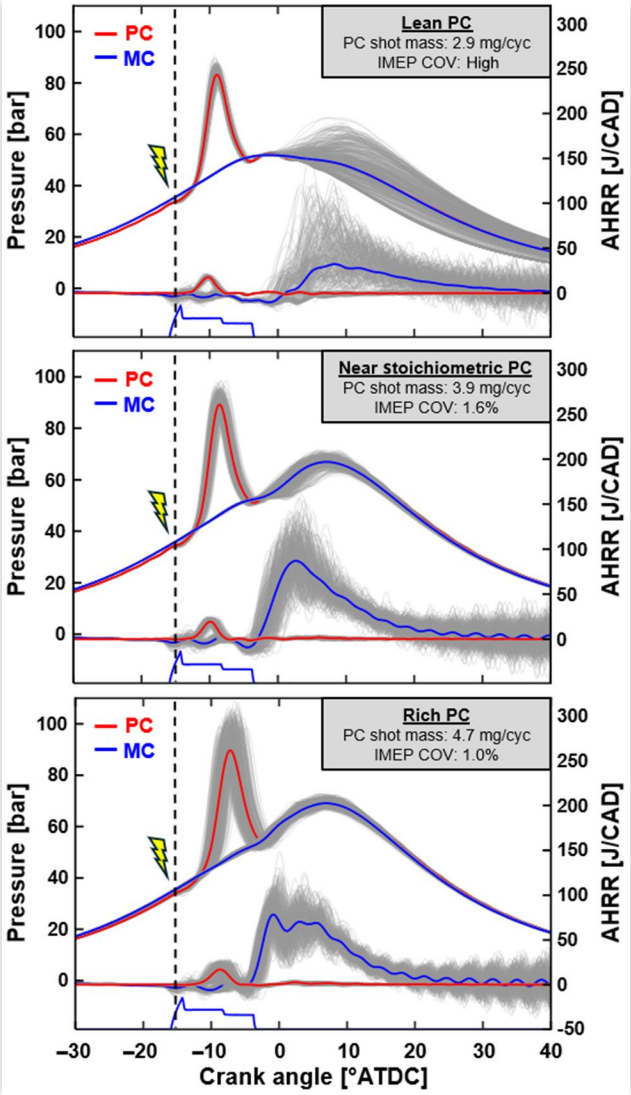


**FIGURE 14** PC spark timing sweep relative to fixed direct injection conditions. Injection timing and PC shot mass are –16°ATDC and 4.3 mg/cyc, respectively.

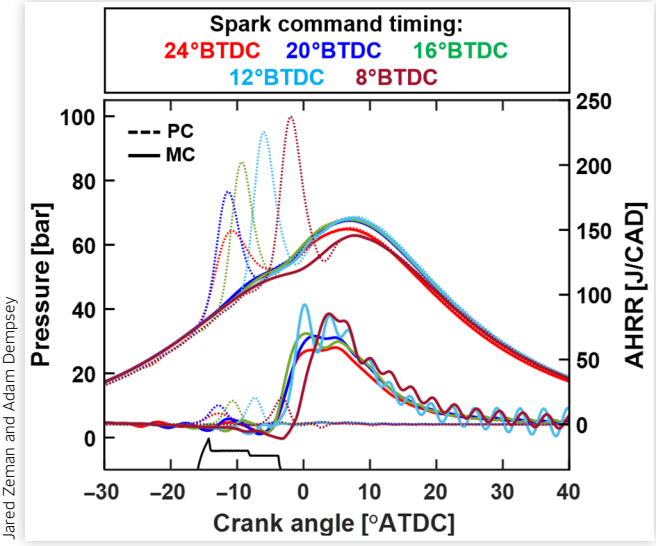


penetrate whereas lean jets have little post-ejection exothermicity and thus are weak ignition sources. These experimental results further allude to the strength of the ignition sources under rich operation due to the inverse relation of PC and MC cyclic variability.

Overall, the combustion efficiency is observed to peak around 98% with CO and UHC emissions levels near 3 g/kW-h–5 g/kW-h. In addition to the potential PC combustion inefficiencies discussed in the previous section, it is suspected that other sources of combustion inefficiencies are formed on the far side of the combustion chamber from the PC (see Figure 3) where the PC jets and spray have the weakest (if any) interaction where spray overmixing and surface impingement are likely to occur. These sprays are likely last to ignite, and their ignition mechanism is not yet fully understood. Based on previous PC-MCC CFD modeling efforts [34, 36], as the jets penetrate the MC, they entrain the relatively cool (–1000 K) bulk gases and consequently drop in temperature rapidly. If the PC jets are to penetrate across the MC uninhibited, it is unlikely that they are hot enough to motivate sufficient ignition of the aforementioned DI sprays. Despite rapid cooling, the jet's momentum is sufficient to entrain/deflect oxidizing reactants and/or burned products as they traverse from one side of the chamber to the other, thus motivating ignition by redirection of ignited sprays. In the absence of strong jet-induced effects, it is suspected that the sprays ignite due to flame propagation from neighboring sprays that have ignited or undergone autoignition as the chamber pressure and temperature rise from other jet-ignited sprays.

Next, the impact of PC combustion timing and DI timing split was evaluated by fixing the commanded injection timing and varying the PC combustion timing. For this study, the PC fueling was fixed at 4.3 mg/cyc, and the main injection was maintained at –16°ATDC. The subsequent ignition trends with varying spark timing are observed in Figures 14 and 15. As discussed in the previous section, the PC equivalence ratio is expected to change under varying spark timing. The PC pressure traces in Figure 14 are reminiscent of the results shown in Figure 9, with the most advanced spark timing of –24°ATDC indicative of a rich combustion process that subsequently improves as the concentration of air in the PC is increased at later timings. The erratic combustion behavior and relatively early timing of the PC jets to the injection timing result in poor ignition quality with high UHC emissions at the earliest timings considered. As the timing retards, the ignition quality improves in response to more favorable PC mixture formations and improved jet–spray timings.

**FIGURE 15** Emissions and engine performance trends with respect to changes in spark timing relative to fixed direct injection conditions. Commanded start of direct injection (SOIc) timing of –16°ATDC and estimated actual start of hydraulic injection (SOI) is illustrated for reference.

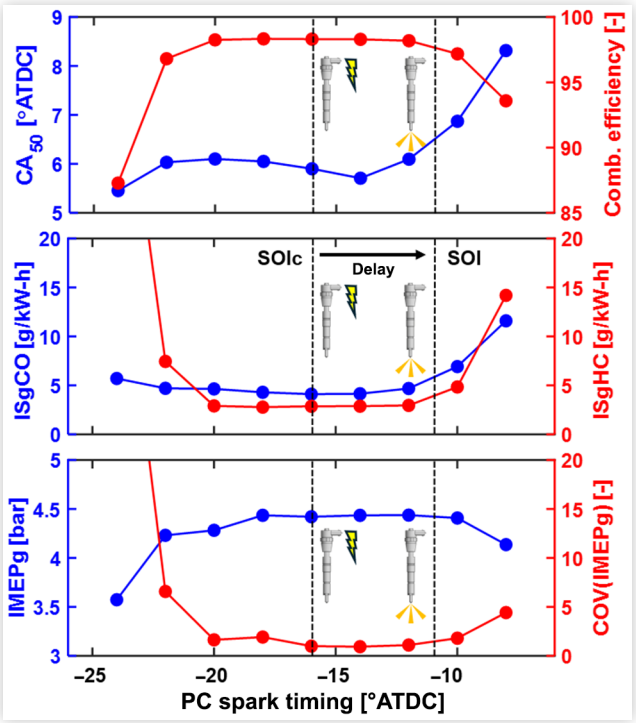


Jared Zeman and Adam Dempsey

At late spark timings, the ignition performance deteriorates as the jets that are beginning to lean out and are too late to reliably ignite the well-established spray nearing the end of injection. As such, an approximate 10 CAD spark timing window of reliable ignition performance of the injected E98 was achieved irrespective of the PC mixture formation at spark timing. These results strongly suggest that the most favorable jet–spray interactions occur when the start of hydraulic injection and start of jet ejection, which generally occurs near the location of peak PC pressure [33, 34], are closely coupled.

Lastly, the impact of PC combustion and DI timing split was again evaluated but now by fixing the PC spark timing and varying the commanded injection timing. For this study, the PC fueling was fixed at 4.3 mg/cyc and commanded spark timing maintained at –15°ATDC. By fixing the PC timing and fueling quantity, PC stoichiometry effects are effectively eliminated for this timing study. The subsequent ignition trends with varying injection timing are observed in Figures 16 and 17.

It is observed in Figure 16 that the earliest injection timings do not ignite until the PC combustion ensues, leading to high overmixing and subsequent poor ignition quality. As the injection timing retards, the combustion phasing also retards, demonstrating an approximate 10 CAD window of reliable ignition performance from the PC and direct control of combustion phasing with injection

**FIGURE 16** Injection timing sweep relative to fixed PC combustion. PC spark timing and shot mass are –15°ATDC and 4.3 mg/cyc, respectively.

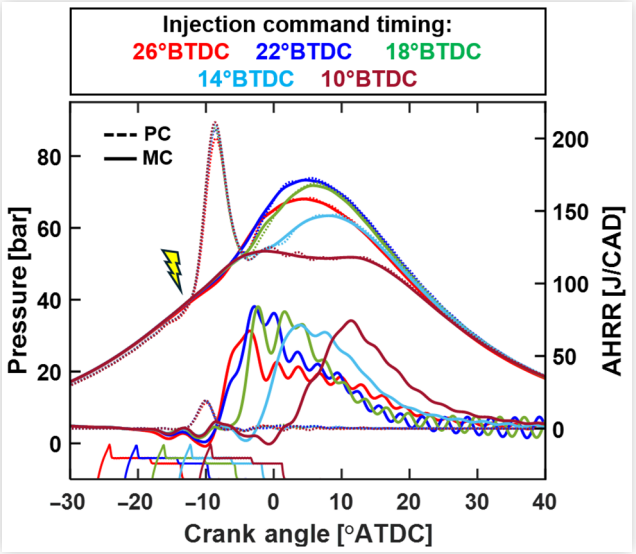


Jared Zeman and Adam Dempsey

command alone. As the spray becomes excessively retarded relative to the PC combustion, the PC jets are completely exhausted and mix out and cool off quickly. As such, the ignition quality rapidly deteriorates and further changes in combustion phasing will require that the PC and DI timing retard together. These results highlight that at the selected light load condition, the energy input from the PC (which is roughly 5% of the total fuel energy input) does not have enough bulk gas heating potential to raise the gas temperature and induce ignition of the E98 fuel. Rather, a jet-induced direct ignition mechanism where the spray and jets are closely coupled to one another and have strong interactions is required for stable combustion. The dependence on a direct ignition mode for this combustion concept is expected to change with load as the thermal boundary conditions increase.

## 3.3. Impact of Cooled External Exhaust Gas Recirculation

For this study, the PC spark timing and DI timing are fixed at –15°ATDC and –16°ATDC, respectively. The PC fueling was gradually decreased in the presence of increasing diluent to maintain stable PC combustion. The recycled exhaust gases were cooled with a conventional coolant-circulated EGR cooler before being recirculated into the intake. Additionally, the intake temperature was maintained at 50°C by modulating the power to the intake heater in the intake system. In essence, any thermal motivation from hot recirculated gases was effectively eliminated to help isolate and evaluate the PC ignition performance. The impact of cooled external EGR on the MC and PC combustion process is illustrated in Figures 18 and 19 and resultant engine performance and emissions are depicted in Figure 20.

**FIGURE 17** Emissions and engine performance trends with respect to changes in direct injection timing relative to fixed PC combustion. Spark timing of –15°ATDC is illustrated for reference.

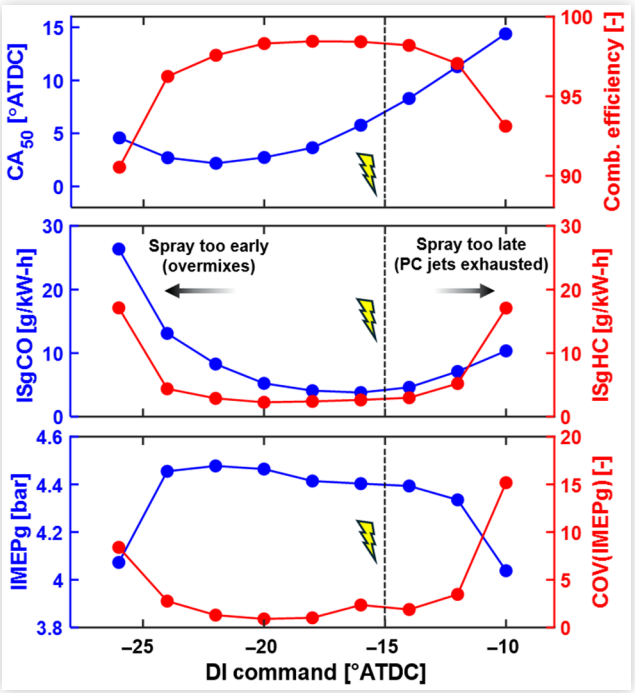


Jared Zeman and Adam Dempsey

**FIGURE 18** Impact of cooled external **e**xhaust gas recirculation. Commanded spark and DI timing is fixed at –15°ATDC and –16°ATDC, respectively.

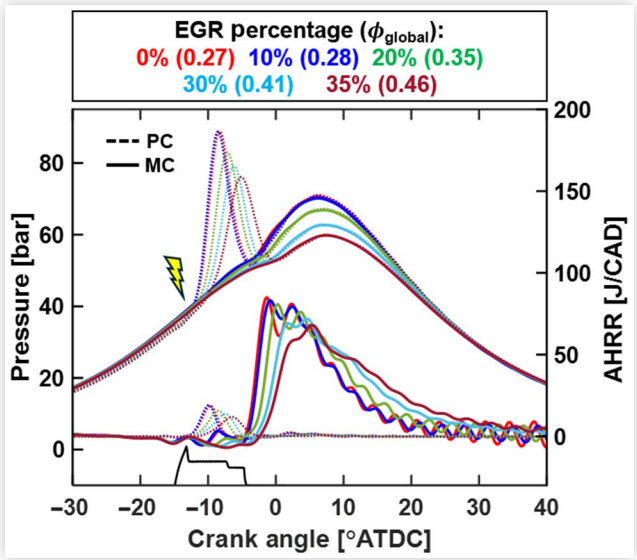


Jared Zeman and Adam Dempsey

**FIGURE 19** Cycle average (solid black) and individual cycles (gray) of PC pressure from under different EGR rates. A PC motoring trace is provided for reference. PC spark timing is fixed at –15°ATDC.

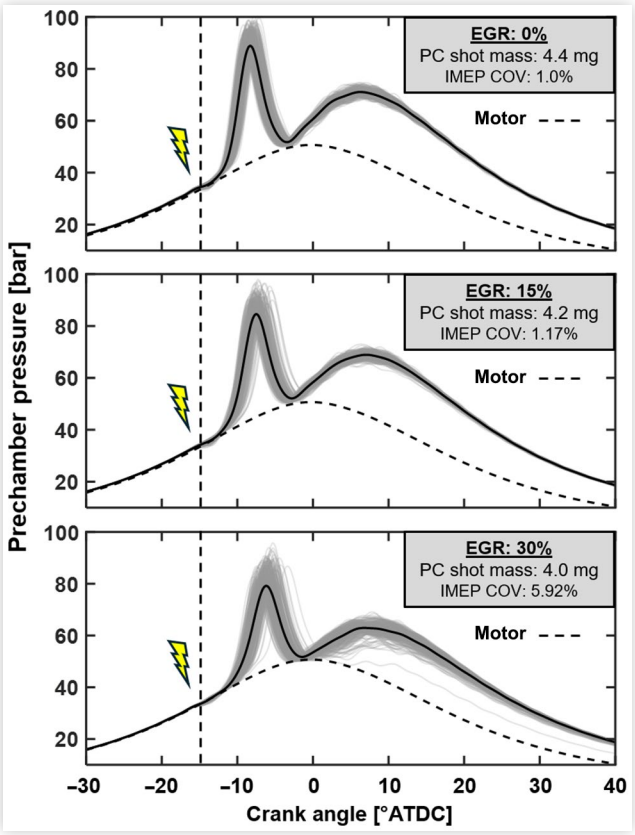


Jared Zeman and Adam Dempsey

**FIGURE 20** Emissions and engine performance trends with cooled external EGR percentage.

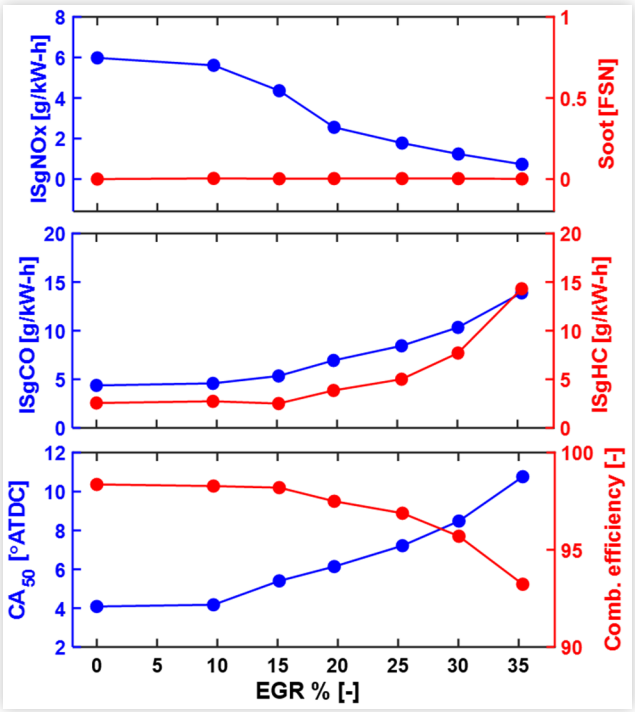


Jared Zeman and Adam Dempsey

The effect of excess diluent on the spark-initiated PC combustion process is readily observed in Figures 18 and 19 as the pressure rise slows and onset of combustion retards with increasing diluent. It is also observed that the MC combustion phasing retards and CO/UHC emissions rise with increasing diluent. Based on the results from Figure 14, the marginal delay in PC combustion is not believed to be solely responsible for the simultaneous deterioration in MC combustion—rather, the reductions in jet quality (lower jet velocities and temperatures) degrade the jet ignition process. With deteriorating jet quality, the initiation of combustion is weakened and the ignition delay increases. Following the ignition delay, spray overmixing and incomplete combustion rise in areas where there is not strong jet-induced ignition, i.e., the far side of the MC from PC. Other combustion inefficiencies likely stem from poor PC combustion in the presence of high dilution. Based on these results and the combustion efficiency trends reported in Figure 20, PC-MCC demonstrates EGR tolerance up to 20%–30% until poor dilution tolerance in the PC degrades the ignition performance substantially. These EGR limits are specific to this operating condition and PC design, but likely serve as a reasonable estimate.

In spite of increasing combustion inefficiencies, thermal NOx emissions decrease in response to increasing EGR percentage, as expected. Interestingly, diffusion combustion of E98 does not demonstrate the classical diesel NOx–soot tradeoff where reductions in NOx by EGR lead to increasing levels of soot [46, 47]. At the selected light load condition, the engine still operates globally lean with plenty of excess oxygen to encourage high local air–fuel ratios of the E98 spray. Ethanol also contains its own oxygen and thus has a lower sooting propensity compared to high carbon intensity [48], even in the presence of excess diluent. Jet-induced diffusion combustion of alcohol fuels in a high dilution environment demonstrates a promising pathway for ultra-low NOx and sootless combustion; however, the lack of dilution tolerance in the PC and subsequent deterioration in ignition quality limits the applicability of such operation. The use of an auxiliary air valve in the PC to purge the combustion residuals would enhance the scavenging and improve PC EGR tolerance, as achieved in dual-mode TJI (DM-TJI) [49, 50]. For the current scope of this work, the use of advanced scavenging strategies will not be investigated further but is regarded as a future strategy to enable high dilution tolerance for PC-MCC.

## 3.4. Comparisons to Diesel Combustion at Matched Phasing

In this final section, comparisons of engine performance and emissions are made between E98 PC-MCC and CDC over a combustion phasing ($CA_{50}$) sweep. Combustion phasing is swept from early (TDC) to late (25°ATDC). The interest in the late combustion timings considered in this study is solely motivated by the need for thermal management of exhaust aftertreatment systems at light load conditions. In this study, combustion phasing is used as a thermal management strategy (as opposed to use of late post injections) to understand the implications of retarded combustion phasing on PC-MCC engine performance, especially when firing the PC into the expansion stroke. For PC-MCC, the relative timing advance between the commanded spark and injection timing is fixed and is maintained throughout the sweep. In other words, as the injection timing retards, the PC spark timing retards equally. For this sweep, the relative advance is 0 CAD, i.e., identical timing. The PC fueling is metered to maintain favorable combustion across the timing sweep based on the results from Figure 9. The relevant PC and DI operating parameters are provided in Table 4.

Comparisons of the E98 PC-MCC and diesel combustion processes over the phasing sweep at select timings are illustrated in Figure 21. At first glance, PC-MCC demonstrates robust control over combustion phasing by simply changing the injection and spark timing command in unison. The jet-induced ignition process maintains a relatively constant ignition delay period and subsequent combustion process over the timing sweep while diesel combustion has varying ignition delay that transitions into partially premixed combustion (PPC) at late timings. The rapid energy release associated with long spray-mixing time is loud and can exceed tolerable engine noise or designed pressure rise rate (PRR) constraints. As such, pilot injections are commonly used in diesel combustion systems at light load conditions to abate excessive PRR. Figure 22 illustrates the effect of pilot injections on diesel combustion in terms of electronic pilot fraction (EPF), or

**TABLE 4** PC-MCC PC and DI operating parameters for combustion phasing sweep. DI start of injection command (electronic) is reported as DI SOIc.

| | $CA_{50}$ [°ATDC] | | | | | | | |
|---|---|---|---|---|---|---|---|---|
| | 0 | 3 | 7 | 10 | 13 | 17 | 20 | 25 |
| PC spark [°ATDC] | –20 | –17 | –13 | –9.5 | –6 | –2 | 0.5 | 4 |
| DI SOIc [°ATDC] | –20 | –17 | –13 | –9.5 | –6 | –2 | 0.5 | 4 |
| PC fuel [mg] | 3.7 | 3.7 | 4.2 | 4.9 | 5.3 | 5.5 | 5.5 | 5.5 |

**FIGURE 21** Combustion phasing sweep ($CA_{50}$) for E98 PC-MCC (top) and conventional diesel combustion (bottom). Note that the AHRR plots for PC-MCC and CDC are scaled differently for viewing purposes.

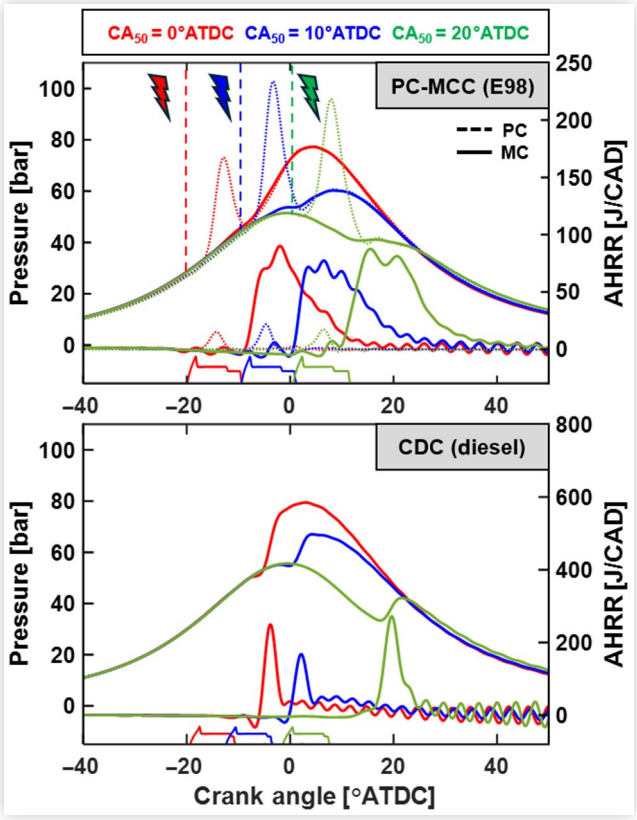


**FIGURE 22** Conventional diesel combustion electronic pilot fraction (EPF) sweep. Pilot advance is fixed 15 CAD before main injection command. CA50 is fixed at −5°ATDC.

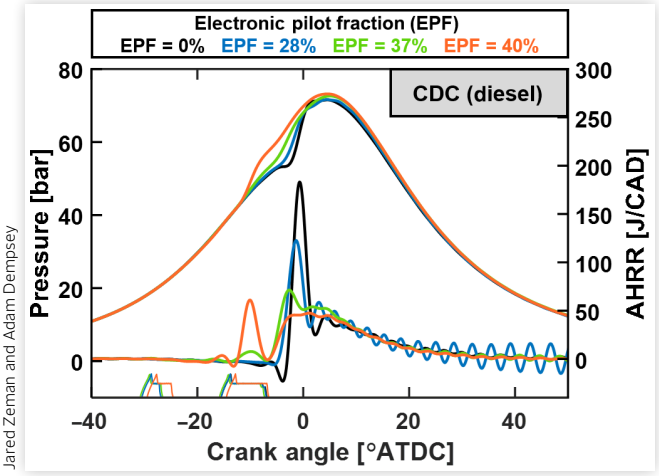


the ratio of energizing time between the pilot and main injections. The efficacy of the pilot injection to reduce the degree of premixed combustion and thus overall PRR/combustion noise is clearly demonstrated from small to large pilot quantities. Despite the low-cetane number of E98, the jet-induced combustion process of PC-MCC does not necessitate the use of a pilot injection to manage PRR at light load conditions. This is favorable as it reduces engine calibration complexity regarding the pilot injection (timing and duration) and reduces the overall number of injection events per cycle, which improves injector longevity, especially when considering the low lubricity content of ethanol. For this study, the diesel phasing sweep was performed with a single injection; however, the salient engine performance and emissions results with pilot injections from Figure 22 will be included for insight in the following analysis.

Relevant engine performance metrics and emissions between E98 PC-MCC and CDC are depicted in Figures 23 and 24, respectively. PC-MCC demonstrates improved gross thermal efficiency and simultaneous reductions in NOx and near-zero soot relative to CDC while maintaining a COV of gross load of less than 2%. The thermal efficiency enhancements and emission benefits are believed to be rooted in the unique fuel properties of ethanol. First, the oxygen content of ethanol allows for higher local air–fuel ratios while its high latent heat of vaporization lowers local mixing temperatures, simultaneously reducing NOx and soot. Lower local flame temperatures also likely result in lower near-wall temperatures and thus reduce heat transfer losses. The enhanced mixing of ethanol also accelerates the burn rate and thus benefits from the efficiency merits of short combustion duration [51–53] in the absence of excessive heat transfer effects due to high PRR. Conversely, the high degree of premixed combustion observed with CDC exacerbates heat transfer losses and is likely a high source of inefficiency. The use of pilot injections with CDC to reduce PRR shows an improvement in thermal efficiency up to roughly 1%.

Included in Figure 23 is an acoustic determination of combustion noise following the work of Shahlari and Ghandhi [54, 55]. The combustion noise is calculated from raw individual cylinder pressure traces with a filter that accounts for noise attenuation from the engine structure as well as the frequency response of human hearing (A-filter), and thus is presented in units of dBA. Occupational noise levels over 85 decibels are considered to be damaging to human hearing by the Occupational Safety and Health Administration (OHSA) [56] and 90 decibels has been used in the past for acceptable combustion-generated noise limits in heavy-duty gasoline CI research [57]. As expected by the inspection of Figure 21, E98 PC-MCC is substantially quieter than single-injection CDC and is within acceptable noise levels of <90 dBA. The use of a pilot injection with CDC helps dampen excessive combustion noise to within the acceptable limits.

Despite reductions in NOx and soot, E98 PC-MCC exhibits nominally higher CO/UHC emissions than CDC with a combustion efficiency that is roughly 98% until combustion phasing exceeds 15°ATDC. To complement

**FIGURE 23** Engine performance metrics at matched combustion phasing for E98 PC-MCC (red) and conventional diesel combustion (black). Diesel combustion with pilot injection is provided for reference.

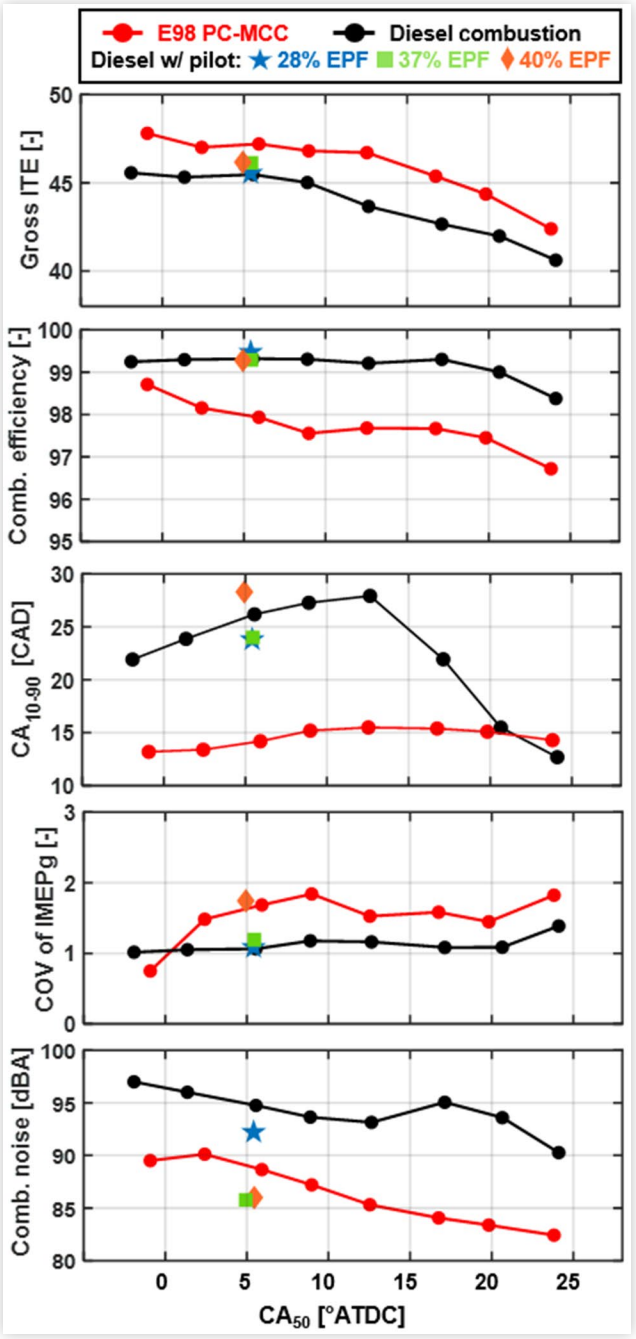


Jared Zeman and Adam Dempsey

**FIGURE 24** Exhaust emissions at matched combustion phasing for E98 PC-MCC (red) and conventional diesel combustion (black). Diesel combustion with pilot injection is provided for reference.

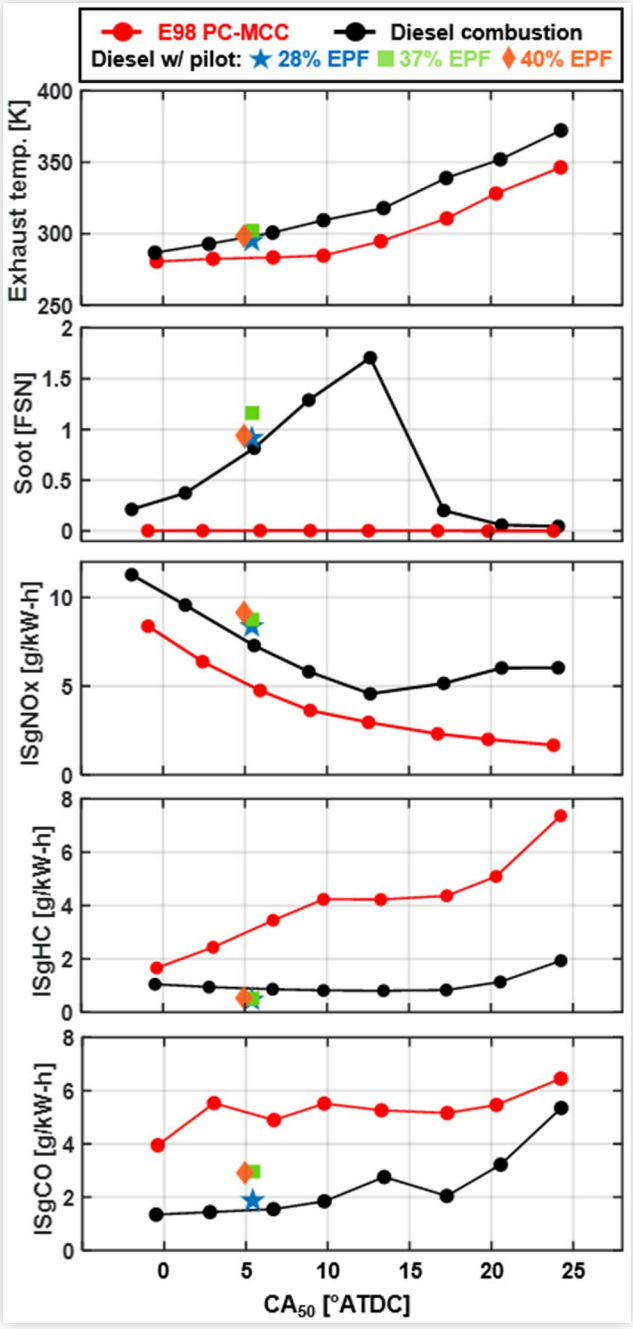


Jared Zeman and Adam Dempsey

**FIGURE 25** Exhaust constituent breakdown for PC-MCC with E98 (red) and diesel combustion (black) at advanced (top) and retarded (bottom) combustion phasing. Note that the bar chart is NOT to scale and is artificially scaled for viewing ease.

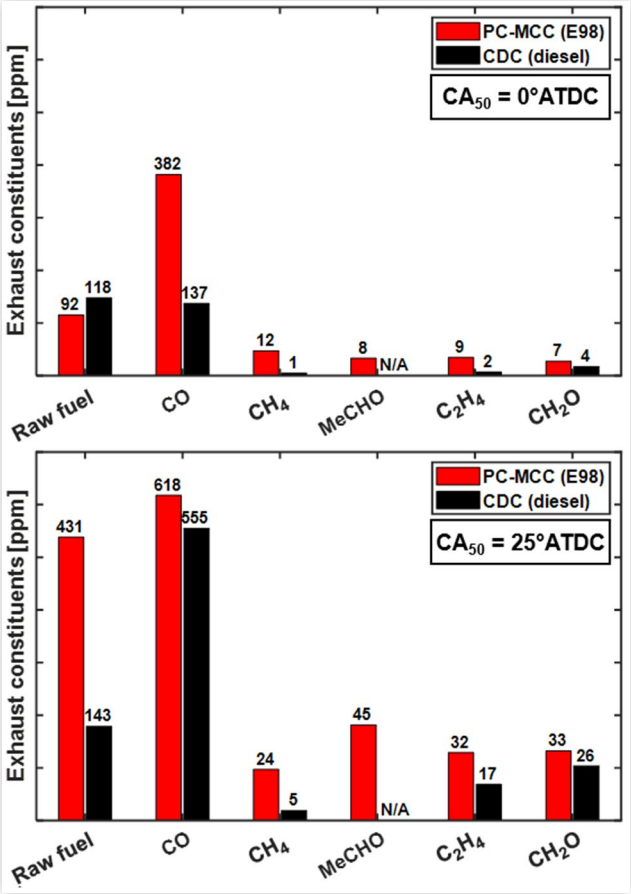


Jared Zeman and Adam Dempsey

the trends observed in Figure 24, Figure 25 depicts an FTIR exhaust speciation for E98 PC-MCC and CDC. The concentration of the individual species is reported in ppm and include raw fuel, i.e., ethanol or diesel, CO, methane ($CH_4$), acetaldehyde (MeCHO), ethylene ($C_2H_4$), and formaldehyde ($CH_2O$). The selected exhaust constituents are specifically geared toward the incomplete combustion of ethanol in which the hydroxyl group (OH) tends to form high concentrations of aldehydes, namely formaldehyde and acetaldehyde. Other byproducts considered are methane and ethylene, which contribute to formaldehyde and acetaldehyde formation in post-flame oxidation reactions [58], respectively. The speciation is provided at 0°ATDC and 25°ATDC to quantify the relative increases in individual species as combustion efficiency begins to drop.

At a $CA_{50}$ of TDC, PC-MCC achieves its highest combustion efficiency and shows diesel-like levels of UHC but at increased CO levels. At a $CA_{50}$ of 25°ATDC, PC-MCC sees a concurrent rise in raw fuel and CO where CDC's combustion inefficiency is largely CO due to PPC-like combustion [59]. An increase in aldehyde emissions is also observed and is roughly proportional to the increase in unburned ethanol. Both combustion chambers are suspected to have sources of UHC and CO emissions. In the MC, the source of UHC's and incomplete oxidation of CO is likely formed away from jet-induced ignition sites where spray overmixing occurs and likely worsens as the in-cylinder conditions deteriorate at late timings. The source of UHC from the PC is believed to follow the results and discussion pertaining to Figures 9 and 10 where raw ethanol slip was observed to increase rapidly at late PC spark timings. These results were conducted with PC combustion only; thus, it is not fully understood if any raw fuel or CO emissions produced by the PC are suitable to be oxidized locally near an established diffusion flame or overmix rapidly and lead to an indefinite source of combustion inefficiency.

It is uncertain to the degree to which each chamber contributes to the observed UHC emissions. At this light load condition, the PC contains roughly 5%–10% of the total fuel energy input, thus any combustion inefficiencies associated with the PC will have a non-negligible influence on the total combustion efficiency. One way to distinguish the predominant source of UHCs experimentally is to use a different fuel source in the PC, e.g., hydrogen or methane, such that UHC emissions can be compared under matched in-cylinder conditions. A gaseous fuel source is preferred such that spray evaporation and wall-wetting effects are eliminated. Hydrogen has great PC SI properties including high laminar flame speeds and short quenching distances [60] that would enable fast PC mixture consumption and low combustion inefficiencies from crevice and near-wall flame quenching. Hydrogen is not directly measured by an FTIR or HFID, thus any reductions in UHC would be used to infer the UHC contributions from the PC under ethanol fueling. If a more quantitative speciation methodology is desired, methane would be a good candidate as it is measurable directly by an FTIR and also contributes to the total UHC measured by an HFID.

# 4. Conclusion

This experimental study involves a preliminary assessment of PC-MCC with E98 fuel in a heavy-duty engine. First, the PC combustion trends were evaluated with respect to relevant PC operating parameters (spark timing, injection timing, injection quantity) in a series of PC-only experiments, i.e., no MC direct-injected fuel. Then, direct-injected fuel was introduced and the ignition assistance trends with PC operating strategy were assessed based on engine performance and emissions. Lastly, engine performance and emissions trends were evaluated relative to conventional diesel combustion at matched combustion phasing. The selected operating point for this

study was a light load (2 bar BEMP), high engine speed (2200 rpm) condition that was representative of a hard-to-ignite scenario where the E98 was completely reliant on the ignition assistance from the PC to attain stable rate-limited combustion. The following conclusions were drawn from this investigation:

1. In this preliminary experimental investigation, PC-MCC exhibits the ability to facilitate robust mixing-controlled combustion of E98 at diesel-like conditions. The conceptual validity of PC-MCC with E98 fuel prompts agnostic applicability to other low-cetane alternatives.
2. Favorable ignition assistance was achieved under slightly rich to rich PC conditions with the PC spark timing closely coupled to the commanded injection timing. The results suggest a ~10 CAD window of operable dwell between the spark and injection timing that achieved good ignition performance.
3. E98 PC-MCC demonstrated improvements in thermal efficiency with simultaneous reduction in NOx and near-zero soot in comparison to diesel combustion. Under appropriate PC operation, PC-MCC achieved a COV of gross load less than 2%.
4. PC-MCC was shown to have EGR tolerance up to 30% before deterioration in the premixed PC combustion process limited further dilution. Advanced scavenging strategies are likely needed to further improve the dilution tolerance of the spark-initiated combustion process in the PC.
5. The combustion efficiency of E98 PC-MCC was limited to ~98%, which is considered to be diesel-like at the selected light load condition. Regardless, there is an impetus to locate the source of said combustion inefficiency. In the PC, the most likely sources of combustion inefficiency are fuel that escapes the PC early in the compression stroke during injection, PC fuel films that are unable to participate in PC combustion, and "cool jet" ejection of unburned PC charge ahead of the expanding flame front during PC combustion. The source of combustion inefficiencies in the MC is limited to incomplete combustion of direct-injected fuel sprays, especially those that have weak interactions with the PC jets.

## Acknowledgements

This material is based upon work supported by the U.S. Department of Energy's Office of Energy Efficiency and Renewable Energy (EERE) under the Award Number DE-EE0009872.

## Contact Information

**Jared Zeman**, corresponding author
jared.zeman@marquette.edu

## Definitions/Abbreviations

**°ATDC** - Degrees after top dead center firing
**AHRR** - Apparent heat release rate
**BDC** - Bottom dead center
**BMEP** - Brake mean effective pressure
**CA50** - Location of 50% burn
**CAD** - Crank angle degree
**CDC** - Conventional diesel combustion
**CI** - Compression ignition
**CRS** - Common rail system
**DI** - Direct injection
**DM-**TJI - Dual-mode turbulent jet ignition
**E98** - Fuel-grade ethanol (2% denaturant by volume)
**EGR** - Exhaust gas recirculation
**EPF** - Electronic pilot fraction
**FSN** - Filter smoke number
**FTIR** - Fourier transform infrared spectrometer
**GDI** - Gasoline direct injection
**HFID** - Heated flame ionization detector
**HPDI** - High-pressure direct injection
**IVC** - Intake valve closure
**MC** - Main chamber
**MCC** - Mixing-controlled combustion
**MJI** - MAHLE jet ignition
**MSP** - Measuring spark plug
**PC** - Prechamber
**PC-**MCC - Prechamber-enabled MCC
**PPC** - Partially premixed combustion
**PRR** - Pressure rise rate
**ROI** - Rate of injection
**SI** - Spark ignition
**SOI** - Start of hydraulic injection
**SOIc** - Commanded start of injection
**TDC** - Top dead center
**TJI** - Turbulent jet ignition
**UHC** - Unburned hydrocarbon

# References


1. ExxonMobil, "Outlook for Energy," accessed January 15, 2023, https://corporate.exxonmobil.com/Energy-and-innovation/Outlook-for-Energy#ExxonMobilsupportstheParisAgreement.
2. Lewandrowski, J., Rosenfeld, J., Pape, D. et al., "The Greenhouse Gas Benefits of Corn Ethanol—Assessing Recent Evidence," *Biofuels* 11 (2020): 361-375.
3. Wang, M., "Biofuel Life-Cycle Analysis with the GREET Model," in *Biofuel Greenhouse Gas Modeling Workshop*, 2011, https://www.epa.gov/renewable-fuel-standard-program/workshop-biofuel-greenhouse-gas-modeling.
4. Dempsey, A., Chowdhury, M., Kokjohn, S., and Zeman, J., "Prechamber Enabled Mixing Controlled Combustion—A Fuel Agnostic Technology for Future Low Carbon Heavy-Duty Engines," SAE Technical Paper 2022-01-0449 (2022), doi:https://doi.org/10.4271/2022-01-0449.
5. Mueller, C. and Musculus, M., "Glow Plug Assisted Ignition and Combustion of Methanol in an Optical DI Diesel Engine," SAE Technical Paper 2001-01-2004 (2001), doi:https://doi.org/10.4271/2001-01-2004.
6. Amezcua, E.R., Kim, K., Rothamer, D., and Kweon, C., "Ignition Sensitivity Analysis for Energy-Assisted Compression-Ignition Operation on Jet Fuels with Varying Cetane Number," SAE Technical Paper 2022-01-0443 (2022), doi:https://doi.org/10.4271/2022-01-0443.
7. Sapra, H.D., Hessel, R., Amezcua, E. et al., "Numerical Modeling and Analysis of Energy-Assisted Compression Ignition of Varying Cetane Number Jet Fuels for High-Altitude Operation," *Journal of Engineering for Gas Turbines and Power* 145, no. 9: 091004, doi:https://doi.org/10.1115/1.4062415/1163118.
8. Sapra, H., Hessel, R., Miganakallu, N. et al., "Computational Fluid Dynamics and Machine Learning-Based Piston-Bowl Optimization for Energy-Assisted Compression Ignition of Low Cetane Number Sustainable Aviation Fuel Blends," *Energy Convers Manag* 300 (2024): 117929.
9. Richards, B., "Methanol-Fueled Caterpillar 3406 Engine Experience in On-Highway Trucks," SAE Technical Paper 902160 (1990), doi:https://doi.org/10.4271/902160.
10. Svensson, E. and Verhelst, S., "Numerical Optimization of Compression Ratio for a PPC Engine Running on Methanol," SAE Technical Paper 2019-01-2168 (2019), doi:https://doi.org/10.4271/2019-01-2168.
11. Svensson, M., Tuner, M., and Verhelst, S., "Low Load Ignitability of Methanol in a Heavy-Duty Compression Ignition Engine," SAE Technical Paper 2022-01-1093 (2022), doi:https://doi.org/10.4271/2022-01-1093.
12. Kolodziej, C., Kodavasal, J., Ciatti, S., Som, S. et al., "Achieving Stable Engine Operation of Gasoline Compression Ignition Using 87 AKI Gasoline Down to Idle," SAE Technical Paper 2015-01-0832 (2015), doi:https://doi.org/10.4271/2015-01-0832.
13. Blumreiter, J., Johnson, B., Zhou, A., Magnotti, G. et al., "Mixing-Limited Combustion of Alcohol Fuels in a Diesel Engine," SAE Technical Paper 2019-01-0552 (2019), doi:https://doi.org/10.4271/2019-01-0552.
14. Kumar, P. and Zhang, Y., "Variable Valve Strategy Evaluation for Low-Load Operation in a Heavy-Duty Gasoline Compression Ignition Engine," *Energies* 15, no. 6 (2022): 2017.
15. Johnston, T. and Dempsey, A., "Mixing-Controlled Compression Ignition with Exhaust Rebreathe on a Heavy-Duty Engine—A CFD Modelling Investigation Comparing Diesel Fuel and Ethanol," in *ASME 2023 ICE Forward Conference*, Pittsburgh, PA, January 16, 2024, https://doi.org/10.1115/ICEF2023-109548.
16. Gainey, B., Yan, Z., Rahimi-Boldaji, M. et al., "On the Effects of Injection Strategy, EGR, and Intake Boost on TSCI with Wet Ethanol," in *ASME 2019 Internal Combustion Engine Division Fall Technical Conference, ICEF 2019*, Chicago, IL, 2020, American Society of Mechanical Engineers (ASME), https://doi.org/10.1115/ICEF2019-7164.
17. Gainey, B., Yan, Z., Gohn, J., Rahimi Boldaji, M. et al., "TSCI with Wet Ethanol: An Investigation of the Effects of Injection Strategy on a Diesel Engine Architecture," SAE Technical Paper 2019-01-1146 (2019), doi:https://doi.org/10.4271/2019-01-1146.
18. Gainey, B., Bhatt, A., Gandolfo, J., Vedpathak, K. et al., "Experimental Comparison of Diesel and Wet Ethanol on an Opposed-Piston Two Stroke (OP2S) Engine," SAE Technical Paper 2023-01-0335 (2023), doi:https://doi.org/10.4271/2023-01-0335.
19. Dempsey, A.B., Curran, S.J., and Wagner, R.M., "A Perspective on the Range of Gasoline Compression Ignition Combustion Strategies for High Engine Efficiency and Low NOx and Soot Emissions: Effects of In-Cylinder Fuel Stratification," *International Journal of Engine Research* 17 (2016): 897-917.
20. Dempsey, A., Walker, N., and Reitz, R., "Effect of Cetane Improvers on Gasoline, Ethanol, and Methanol Reactivity and the Implications for RCCI Combustion," *SAE Int. J. Fuels Lubr.* 6, no. 1 (2013): 170-187, doi:https://doi.org/10.4271/2013-01-1678.
21. Chowdhury, M. and Dempsey, A., "Inverted Reactivity Controlled Compression Ignition (iRCCI) with Methanol Fuel & Reactivity Enhancers," SAE Technical Paper 2022-01-0464 (2022), doi:https://doi.org/10.4271/2022-01-0464.
22. Kokjohn, S.L., Hanson, R.M., Splitter, D.A. et al., "Fuel Reactivity Controlled Compression Ignition (RCCI): A Pathway to Controlled High-Efficiency Clean Combustion," *International Journal of Engine Research* 12 (2011): 209-226.
23. Dempsey, A., Curran, S., and Reitz, R., "Characterization of Reactivity Controlled Compression Ignition (RCCI) Using Premixed Gasoline and Direct-Injected Gasoline

with a Cetane Improver on a Multi-Cylinder Engine," *SAE Int. J. Engines* 8, no. 2 (2015): 859-877, doi:https://doi.org/10.4271/2015-01-0855.

24. Zheng, Z., Chen, P., Zhang, F. et al., "Experimental Study on the Effect of the Thermal Barrier Coated (TBC) Piston on Combustion of Gasoline Compression Ignition (GCI)," *Appl. Therm. Eng.* 217 (2022): 119068.
25. Yan, Z., Levi, A., Zhang, Y., Sellnau, M. et al., "A Numerical Evaluation and Guideline for Thermal Barrier Coatings on Gasoline Compression Ignition Engines," *International Journal of Engine Research* 24, no. 5 (2023): 2206-2222, doi:https://doi.org/10.1177/14680874221114534.
26. Babu, A., Koutsakis, G., Kokjohn, S., and Andrie, M., "Experimental and Analytical Study of Temperature Swing Piston Coatings in a Medium-Duty Diesel Engine," *SAE Int. J. Adv. & Curr. Prac. in Mobility* 5, no. 1 (2023): 235-248, doi:https://doi.org/10.4271/2022-01-0442.
27. Dong, Y., Kaario, O., Hassan, G. et al., "High-Pressure Direct Injection of Methanol and Pilot Diesel: A Non-Premixed Dual-Fuel Engine Concept," *Fuel* 277 (2020): 117932.
28. Frankl, S., Gleis, S., Karmann, S. et al., "Investigation of Ammonia and Hydrogen as $CO_2$-Free Fuels for Heavy Duty Engines Using a High Pressure Dual Fuel Combustion Process," *International Journal of Engine Research* 22 (2020): 3196-3208.
29. Gleis, S., Frankl, S., Waligorski, D., Prager, D. et al., "Investigation of the High-Pressure-Dual-Fuel (HPDF) Combustion Process of Natural Gas on a Fully Optically Accessible Research Engine," SAE Technical Paper 2019-01-2172 (2019), doi:https://doi.org/10.4271/2019-01-2172.
30. McTaggart-Cowan, G., Mann, K., Huang, J., Singh, A. et al., "Direct Injection of Natural Gas at Up to 600 Bar in a Pilot-Ignited Heavy-Duty Engine," *SAE Int. J. Engines* 8, no. 3 (2015): 981-996, doi:https://doi.org/10.4271/2015-01-0865.
31. Kammel, G., Mair, F., Zelenka, J., Lackner, M. et al., "Simulation Based Predesign and Experimental Validation of a Prechamber Ignited HPDI Gas Combustion Concept," SAE Technical Paper 2019-01-0259 (2019), doi:https://doi.org/10.4271/2019-01-0259.
32. Zelenka, J., Kammel, G., Wimmer, A., Bärow, E. et al., "Analysis of a Prechamber Ignited HPDI Gas Combustion Concept," SAE Technical Paper 2020-01-0824 (2020), doi:https://doi.org/10.4271/2020-01-0824.
33. Dempsey, A.B., Zeman, J., and Wall, M., "A System to Enable Mixing Controlled Combustion with High Octane Fuels Using a Prechamber and High-Pressure Direct Injector," *Front. Mech. Eng.* 7 (2021): 7.
34. Zeman, J., Yan, Z., Bunce, M. et al., "Assessment of Design and Location of an Active Prechamber Igniter to Enable Mixing-Controlled Combustion of Ethanol in Heavy-Duty Engines," *International Journal of Engine Research* 24, no. 9 (2023): 4226-4250, doi:https://doi.org/10.1177/14680874231185421.
35. Zeman, J. and Dempsey, A., "Characterization of Flex-Fuel Prechamber Enabled Mixing-Controlled Combustion (PC-MCC) with Gasoline/Ethanol Blends at High Load," *J. Eng. Gas Turbines Power.* 146, no. 8 (2024): 081015.
36. Zeman, J. and Dempsey, A., "Numerical Investigation of Equivalence Ratio Effects on Flex-Fuel Mixing Controlled Combustion Enabled by Prechamber Ignition," *Appl. Therm. Eng.* 249 (2024): 123445.
37. Dempsey, A.B., Seiler, P.J., and Johnson, S., "Comparison of Cylinder Pressure Measurements on a Heavy-Duty Diesel Engine Using a Switching Adapter," *J. Eng. Gas Turbines Power.* 141, no. 8 (2019): 081014, doi:https://doi.org/10.1115/1.4043408.
38. Higgins, B., Siebers, D., and Aradi, A., "Diesel-Spray Ignition and Premixed-Burn Behavior," SAE Technical Paper 2000-01-0940 (2000), doi:https://doi.org/10.4271/2000-01-0940.
39. Heywood, J., *Internal Combustion Engine Fundamentals*, 2nd ed. (McGraw-Hill, New York, 2019), accessed April 1, 2021, https://www.mheducation.com/highered/product/internal-combustion-engine-fundamentals-2e-heywood/9781260116106.html.
40. Hlaing, P., Silva, M., Marquez, M.E. et al., "Estimates of the Air-Fuel Ratio at the Time of Ignition in a Pre-Chamber Using a Narrow Throat Geometry," *International Journal of Engine Research* 24 (2021): 622-638, doi:https://doi.org/101177/14680874211059148.
41. Hlaing, P., Echeverri Marquez, M., Singh, E., Almatrafi, F. et al., "Effect of Pre-Chamber Enrichment on Lean Burn Pre-Chamber Spark Ignition Combustion Concept with a Narrow-Throat Geometry," SAE Technical Paper 2020-01-0825 (2020), doi:https://doi.org/10.4271/2020-01-0825.
42. Balmelli, M., Rogers, D., Hilfiker, T. et al., "Method for Pressure Trace Based Thermodynamic Analysis of Pre-Chamber Combustion," *Energy Convers Manag* 312 (2024): 118561.
43. Kawabe, T., Inoue, K., Mori, K. et al., "Mechanism of the Reduction in Afterburning and Thermal Efficiency Improvement with Highly Oxygenated Fuels in Diesel Combustion," *International Journal of Engine Research* 24 (2023): 4362-4372, doi:https://doi.org/101177/14680874231197880.
44. Thelen, B.C. and Toulson, E., "A Computational Study of the Effects of Spark Location on the Performance of a Turbulent Jet Ignition System," SAE Technical Paper 2016-01-0608 (2016), doi:https://doi.org/10.4271/2016-01-0608.
45. Rajasegar, R., Niki, Y., García-Oliver, J.M. et al., "Fundamental Insights on Ignition and Combustion of Natural Gas in an Active Fueled Pre-Chamber Spark-Ignition System," *Combust Flame* 232 (2021): 111561.
46. Kitamura, T., Ito, T., Senda, J. et al., "Mechanism of Smokeless Diesel Combustion with Oxygenated Fuels Based on the Dependence of the Equivalence Ration and Temperature on Soot Particle Formation," *International Journal of Engine Research* 3 (2002): 223-248.
47. Kitamura, Y., Mohammadi, A., Ishiyama, T., and Shioji, M., "Fundamental Investigation of NOx Formation in Diesel

Combustion under Supercharged and EGR Conditions," SAE Technical Paper 2005-01-0364 (2005), doi:https://doi.org/10.4271/2005-01-0364.

48. Gross, J., Chowdhury, M., Dempsey, A., and Allen, C., "Soot Formation and Ignition Characteristics of Ethanol/Gasoline Blends in a Rapid Compression Machine," SAE Technical Paper 2023-01-0385 (2023), doi:https://doi.org/10.4271/2023-01-0385.
49. Atis, C.A.A., Ayele, Y., Stuecken, T. et al., "Effect of Pre-Chamber Scavenging Strategy on EGR Tolerance and Thermal Efficiency of Pre-Chamber Turbulent Jet Ignition Systems," *International Journal of Engine Research* 24 (2022): 1938-1960, doi:https://doi.org/101177/14680874221105162.
50. Atis, C., Chowdhury, S., Ayele, Y., Stuecken, T. et al., "Ultra-Lean and High EGR Operation of Dual Mode, Turbulent Jet Ignition (DM-TJI) Engine with Active Pre-Chamber Scavenging," SAE Technical Paper 2020-01-1117 (2020), doi:https://doi.org/10.4271/2020-01-1117.
51. Caton, J.A., "The Thermodynamic Characteristics of High Efficiency, Internal-Combustion Engines," *Energy Convers Manag* 58 (2012): 84-93.
52. Caton, J.A., "Combustion Phasing for Maximum Efficiency for Conventional and High Efficiency Engines," *Energy Convers Manag* 77 (2014): 564-576.
53. Wissink, M.L., Splitter, D.A., Dempsey, A.B. et al., "An Assessment of Thermodynamic Merits for Current and Potential Future Engine Operating Strategies," *International Journal of Engine Research* 18 (2017): 155-169.
54. Shahlari, A.J., Kurtz, E., Hocking, C. et al., "Correlation of Cylinder Pressure–Based Engine Noise Metrics to Measured Microphone Data," *International Journal of Engine Research* 16 (2014): 829-850, doi:https://doi.org/101177/1468087414552831.
55. Shahlari, A.J., Hocking, C., Kurtz, E., and Ghandhi, J., "Comparison of Compression Ignition Engine Noise Metrics in Low-Temperature Combustion Regimes," *SAE Int. J. Engines* 6, no. 1 (2013): 541-552, doi:https://doi.org/10.4271/2013-01-1659.
56. Occupational Safety and Health Administration, "Occupational Noise Exposure—Overview," accessed September 8, 2024, https://www.osha.gov/noise.
57. Cung, K., Bitsis, D.C., Miwa, J., Smith, E. et al., "Investigation of Gasoline Compression Ignition (GCI) Combustion in a High Compression-Ratio Heavy-Duty Single-Cylinder Diesel Engine," SAE Technical Paper 2021-01-0495 (2021), doi:https://doi.org/10.4271/2021-01-0495.
58. Zarante, P.H.B. and Sodré, J.R., "Comparison of Aldehyde Emissions Simulation with FTIR Measurements in the Exhaust of a Spark Ignition Engine Fueled by Ethanol," *Heat and Mass Transfer* 54 (2018): 2079-2087.
59. Ekoto, I.W., Colban, W.F., Miles, P.C., Park, S. et al., "UHC and CO Emissions Sources from a Light-Duty Diesel Engine Undergoing Dilution-Controlled Low-Temperature Combustion," *SAE Int. J. Engines* 2, no. 2 (2009): 411-430, doi:https://doi.org/10.4271/2009-24-0043.
60. Jung, Y., Lee, M.J., and Kim, N. Il, "Direct Prediction of Laminar Burning Velocity and Quenching Distance of Hydrogen-Air Flames Using an Annular Stepwise Diverging Tube (ASDT)," *Combust Flame* 164 (2016): 397-399.